Hedgehog signaling controls progenitor differentiation timing

Authors: Megan Rowton[1], Andrew D. Hoffmann[1], Carlos Perez-Cervantes[1], Suzy Hur[1], Nikita Deng[1], Emery Lu[1], Jessica Jacobs-Li[1], Jeffrey D. Steimle[1], Xinan Holly Yang[1], Alexander Guzzetta[1], Sonja Lazarevic[1], Chul Kim[1], Shuhan Yu[1], Mervenaz Koska[1], Erika Hanson[1], Sunny Sun-Kin Chan[2], Daniel J. Garry[2], Kohta Ikegami[1], Michael Kyba[2], Ivan P. Moskowitz[1*]

Affiliations:

1. Departments of Pediatrics, Pathology, and Human Genetics, The University of Chicago, Chicago, Illinois, United States of America

2. Lillehei Heart Institute, University of Minnesota, Minneapolis, MN 55455, USA; Department of Pediatrics, University of Minnesota, Minneapolis, MN 55455, USA

[*] indicates corresponding author: imoskowitz@peds.bsd.uchicago.edu

Key words: Hedgehog signaling, differentiation timing, progenitor, GLI, cardiomyocyte, neuron

Abstract

Hedgehog (Hh) signaling acts as a developmental morphogen that contributes to the diversification of cell fates and tissue patterning in multiple embryonic contexts, as well as regulating the proliferation of adult tissue stem cells[1-9]. Here, we report a novel function of Hh signaling GLI transcription factors (TFs) in directly governing the timing of cellular differentiation, independent of a role in specification or proliferation. Disruption of active Hh signaling in the embryo resulted in reduced expression of a progenitor-specific transcription factor network and the inappropriate activation of cardiac differentiation-specific gene expression programs. Expression of the activating Hh transcription factor, GLI1, a marker and effector of active Hh signaling, is correlated with stem and progenitor states during the differentiation of all three germ layers in mouse and human. Transient induction of GLI1 in mouse embryonic stem cell (mESC)-derived cardiac and neural progenitors delayed the onset of the cardiomyocyte and neuron differentiation programs, respectively, while activating progenitor-specific gene expression. GLI1 expression in cardiac progenitors promoted a shift in chromatin accessibility towards a progenitor-like profile at distal regulatory elements near Hh-dependent genes. Manipulating the balance of active to repressive GLI TF predominance unveiled a molecular switch that determined the activity patterns of progenitor-specific distal *cis*-regulatory elements *in vitro* and *in vivo*. Overriding this switch through forced expression of a repressive GLI TF in cardiac progenitors *in vivo* caused precocious cardiomyocyte differentiation and Congenital Heart Disease (CHD). Our data suggest that a GLI TF switch at distal regulatory elements maintains progenitor cell status and inhibits premature differentiation through the activation and maintenance of a progenitor-specific regulatory network, thus controlling

progenitor differentiation timing. We propose a novel molecular paradigm for progenitor maintenance in diverse cellular contexts by signal-dependent TFs with implications for organ development, regenerative potential, and Hh-driven cancers.

Main text

Hh signaling is active in the progenitor cells of many developing and regenerative organs, where Hh-dependent GLI TFs direct embryonic tissue patterning and control proliferation rate (recently reviewed in refs. 8-9). Hh signaling is effected by the nuclear accumulation of activating GLI TFs (GLI^A TFs: GLI1, $GLI2^A$, $GLI3^A$) at the expense of repressive GLI TFs (GLI^R TFs: $GLI2^R$, $GLI3^R$) in cells receiving Hh signaling ligands, including *Sonic*, *Indian*, and *Desert Hedgehog*[10-23]. *Sonic Hedgehog* (*Shh*) signaling is required for the morphogenesis of critical cardiac structures[24-26]. The vertebrate heart forms from two spatially distinct pools of cardiac progenitors that differentiate at different stages - the first heart field (FHF), which differentiates early and forms the primitive heart tube (HT), and the second heart field (SHF), which differentiates later after migrating into the HT to form cardiac structures critical for mammalian cardiopulmonary circulation, such as the pulmonary artery and atrial septum[27]. SHH ligand released from the pulmonary endoderm activates GLI^A TFs specifically in adjacent SHF cardiac progenitors[24-26], not in the HT itself. The juxtaposition of Hh-signal receiving SHF cardiac progenitors (SHF; Fig. 1a, blue region) adjacent to differentiated FHF cardiomyocytes within the HT (Fig. 1a, red region) provides a unique system for investigating the spatiotemporal regulation of cellular differentiation.

We investigated the molecular consequences of GLI^A activation in posterior SHF (pSHF) cardiac progenitors. We defined GLI^A-dependent gene expression in the pSHF by performing transcriptional profiling of the pSHF microdissected from *Shh* mutant ($Shh^{-/-}$) and littermate control ($Shh^{+/+}$) mouse embryos at E10.5. RNA-seq and confirmation by qPCR or *in situ* hybridization revealed downregulation of many genes expressed in embryonic mesoderm or cardiac progenitors[25,28-33], but not in the heart, such as *Foxf1*, *Wnt2b*, *Snai1,* and *Osr1* and *Gli1*, the Hh signaling-dependent activating GLI TF (Fig. 1b, Extended Data Fig. 1a-d, f, g). Interestingly, upregulated genes in the $Shh^{-/-}$ pSHF included cardiomyocyte differentiation products such as *Myl3*, *Tnni3* and *Nppa*, all of which are absent from wild type cardiac progenitors (Fig. 1b, Extended Data Fig. 1a-b, e), suggesting that Hh signaling activates cardiac progenitor gene expression and represses cardiac differentiation gene expression. We therefore defined all genes with differential expression between the SHF progenitors and differentiated HT by performing transcriptional profiling in wild type E10.5 embryos, and compared the stage-specific genes to genes dysregulated in the $Shh^{-/-}$ pSHF. Hh-activated genes, downregulated in the $Shh^{-/-}$ pSHF, were enriched in pSHF progenitors compared with the HT, whereas Hh-repressed genes, upregulated in the $Shh^{-/-}$ pSHF, were enriched in the differentiated HT compared with the pSHF (Fig. 1c). Gene Ontology (GO) analysis of Hh-activated genes identified Hh-related terms including “smoothened signaling” and progenitor-specific developmental terms including “pattern formation”, “morphogenesis”, and “regionalization,” whereas GO analysis of Hh-repressed genes identified terms associated with cardiomyocyte differentiation, including “muscle cell differentiation”, “myofibril assembly”, “sarcomere”, “myofibrils”, and “cardiac muscle tissue development”

(Fig. 1d). Together, these results indicated that Hh signaling was required for active cardiac progenitor gene expression and for preventing cardiomyocyte differentiation gene expression in pSHF progenitors.

We sought to systematically determine whether our observations in the pSHF reflected a broader correlation of active Hh signaling with progenitor versus differentiated status across diverse developmental contexts[14,34-38]. Using *Gli1* expression as a marker of active Hh signaling[39-42], we assessed Hh signaling activity dynamics during the differentiation of several mouse and human tissues representing all three developmental germ layers, using publicly available RNA-seq datasets[43] (Extended Data Tables 1-2). We binned human and mouse tissue and cell RNA-seq datasets first according to developmental stage (stem, progenitor and differentiated), whereby all embryonic and *in vitro* differentiation-derived intermediate samples were classified as progenitors and all adult and *in vitro* differentiation-derived terminal samples were classified as differentiated. As cellular differentiation progressed from the stem cell stage to the progenitor stage to terminally differentiated cell types, we observed a consistent decrease in *Gli1* expression ranking in all mouse and human differentiation series analyzed, irrespective of cellular germ layer of origin (Fig. 1e, Extended Data Fig. 2a-b). In contrast, *Gapdh* expression ranking remained consistently among the top 10% of genes expressed during the course of cellular differentiation. We next identified all genes differentially expressed between the stem or progenitor stages and the differentiated cell stage for each germ layer. *Gli1* was highly differentially expressed in all mouse and human germ layer differentiation series, demonstrating higher expression in the stem cell stage than the differentiated cell stage (Fig. 1f, Extended Data Fig. 2c-d). GO term analysis of genes more highly expressed in

the progenitor state than the differentiated state identified progenitor-associated terms, including “DNA replication” and “cell cycle,” and identified the Hh-related terms “Hedgehog signaling pathway” and “Basal cell carcinoma” (Fig. 2e). These results confirm that Hh signaling activity and GLI^{A} expression is generally highest in stem cell states followed by step-wise reduction in progenitor and then differentiated cell states in developing cell types from multiple germ layers in mammalian species.

The consistent association of high Hh signaling activity with stem/progenitor states and the replacement of a progenitor gene expression program with a differentiation gene expression program in the *Shh* mutant pSHF suggested that Hh signaling might normally limit the progression of cellular differentiation in multiple developmental contexts. We investigated Hh-dependent differentiation control in directed differentiation assays of mouse embryonic stem cells (mESCs) *in vitro*. A time course of mESC differentiation from stem cells (Day 0; D0) into cardiomyocytes (D12) was confirmed by activation of cardiac progenitor markers *Tbx5, Nkx2-5* and *Isl1* at the cardiac progenitor stage (D4-6) as well as expression of cardiac differentiation product *cardiac TroponinT* (cTnT) and the presence of beating foci of cardiomyocytes at differentiation stages (D8-12) (Figure 2a-h; Extended Data Fig. 3b-d) [44]. Active Hh signaling was observed in stem cells and early mesoderm (D0 to D2), based on the expression of Hh targets *Gli1* and *Ptch1*[38-40] and the predominance of GLI^{A} (GLI1, $GLI3^{A}$) protein abundance over GLI^{R} ($GLI3^{R}$) (Extended Data Fig. 3e-i). In contrast, cardiac progenitors and differentiated cardiomyocytes (D8-12) demonstrated an absence of active Hh signaling, based on a reduction of *Gli1* and *Ptch1* expression and a switch to GLI^{R} predominance over GLI^{A}. Thus, quantification of the relative protein abundances of GLI^{A} to GLI^{R} indicated that a transition from active Hh

signaling to inactive Hh signaling occurred coincident with the onset of cardiomyocyte differentiation (Extended Data Fig. 3j).

We hypothesized that the transition from active Hh signaling and predominance of GLI^A TFs to inactive Hh signaling and predominance of GLI^R TFs was required to promote cardiomyocyte differentiation. We predicted that modeling the transient exposure to active Hh signaling experienced by pSHF cardiac progenitors using induced GLI^A expression may inhibit cardiomyocyte differentiation. To mimic transient exposure to active Hh signaling, we developed a doxycycline-inducible GLI1 overexpression (GLI1 OE) mESC line. This system permitted us to directly stimulate expression of the GLI^A TF GLI1, bypassing upstream Hh signaling components and avoiding GLI2/3 isoform switching. Doxycycline treatment for 24 hours in cardiac progenitor stage cells (D5-6) resulted in 70-fold induction of *Gli1* transcript and GLI1 protein (Fig. 2a, Extended data Fig. 4a) and of the SHF Hh target genes *Foxf1, Foxd1, Foxf2, Osr1* and *Ptch1* within 24 hours (Fig. 2b, Extended Data Fig. 4b-c), confirming that GLI1 OE leads to the activation of known Hh signaling targets[45-48] including a TF network similar to the Hh-driven pSHF network[26] (Fig. 2b, Extended Data Fig. 4b-c). Strikingly, transient GLI1 overexpression in cardiac progenitors (GLI1 OE) inhibited cardiomyocyte differentiation, reflected in a significant reduction in the intensity and proportion of cells expressing cardiac troponin (cTnT) and in the number of beating cardiomyocyte foci at D8, compared to untreated control cells (Fig. 2c-e, Extended Data Fig. 4d). By D12 of differentiation, however, the number of beating foci and cTnT expression became indistinguishable between GLI1 OE cells and control cells (Fig. 2f-h, Extended Data Fig. 4d). These observations indicated that

transient activation of Hh signaling in cardiac progenitors delayed cardiac differentiation, but did not abrogate cardiac differentiation potential or alter cell fate.

We investigated the effect of transient GLI1 OE in cardiac progenitors on the progenitor and differentiation gene expression programs in a temporal series of differentiation stages: cardiac progenitors (D6), early cardiomyocytes (D8) and late cardiomyocytes (D12). GLI1 OE caused a rapid and global increase in the expression of progenitor and mesoderm-specific genes, and a sharp decrease in the expression of cardiomyocyte differentiation genes at D6, such that GLI1 OE and control replicate transcriptomes were clearly segregated with hierarchical clustering (Fig. 2i, Extended Data Fig. 5a-b). GO terms associated with genes induced by GLI1 at D6 included progenitor terms such as “developmental programs” and “cell division”, while GO terms associated with genes down-regulated by GLI1 OE included differentiation terms such as “differentiation”, “cardiomyopathy” and “the sarcomere” (Fig. 2i, Extended Data Fig. 5b). After doxycycline was removed from the media, differentiation proceeded and both progenitor- and differentiation-specific gene expression levels normalized over time. By D12, GLI1 OE and control transcriptomes no longer segregated based on doxycycline treatment (Extended Data Fig. 5a). The number of differentially expressed genes (log_2FC ≥ 1.5; FDR ≤ 0.05) decreased from 1,652 at D6 to 78 by D12. The fold changes of developmental and cardiomyocyte genes dysregulated between GLI1 OE and control cells at D6 decreased over time (Extended Data Fig. 5c), such that by D12, expression levels of progenitor-specific genes such as *Gli1*, *Foxf1* and *Bra* and of cardiomyocyte differentiation genes *Tnnt2*, *Myh6* and *Hand2* in GLI1 OE cells were similar to control cells (Extended Data Fig. 5d-e). GO analysis performed on the 78 genes dysregulated at D12

did not reveal terms associated with cardiac specification (data not shown), confirming that transient GLI1 OE in cardiac progenitors does not alter cell fate decisions within cardiac sub-lineages. Collectively, these results suggested that transient GLI^A expression in cardiac progenitors temporarily prevented differentiation by up-regulating genes characteristic of progenitor functions and down-regulating genes characteristic of cardiomyocyte differentiation.

Given the widespread deployment of Hh signaling during development, we hypothesized that GLI1-induced differentiation delay in cardiac progenitors may reflect a paradigm deployed in other developmental contexts. During vertebrate central nervous system (CNS) development, a Hh gradient specifies distinct classes of neurons[7,49-51]. To investigate whether transient Hh signaling also controls neuron differentiation timing, we utilized an mESC-based model of neuronal differentiation[52-53] (Extended Data Fig. 6a). Differentiating mESCs express neural progenitor markers including *Sox1, Nestin* and *Pax6* from D4, consistent with previous work[54] (Extended Data Fig. 6b). The pan-neuron marker Class III β-tubulin (*Tubb3/TUJ1*)[55] was initially expressed at D6 and increased dramatically by D8, confirming *in vitro* differentiation of immature neurons (Extended Data Fig. 6b). We next assessed baseline Hh signaling during neuron differentiation. Active Hh signaling, reflected by *Gli1, Ptch1* and *Hhip* expression, was detected throughout most of the differentiation trajectory, however, *Gli1*/GLI1 expression was lowest during the transition from the neural progenitor stage to early differentiated neurons (D3-5; Extended Data Fig. 6c-d), suggesting that removal of Hh signaling may be permissive for the transition of neuronal progenitors to *Tubb3*-expressing differentiating neurons.

We transiently increased GLI^A expression in neuronal progenitors *in vitro* in the doxycycline-inducible GLI1 overexpression (GLI1 OE) mESC line to assess the effect of hyperactivation of GLI^A on neuronal differentiation (Fig. 3a). We induced GLI1 expression in neural progenitors (D3-5) and evaluated the effect on neuronal differentiation morphology and on the expression of pan-neuronal differentiation markers. Doxycycline treatment caused a 25-fold increase in *Gli1* expression by the end of treatment, which then subsided to baseline levels by 24 hours post-treatment (Fig. 3b, Extended Data Fig. 6e). In control cells, axons spanning two or more clusters of neurospheres or neural rosettes (radially organized neural precursors characteristic of *in vitro* neuron differentiation) were observed at D5. Upon GLI1 OE, axon emergence at D5 was significantly reduced (Fig. 3d), although the number of neural rosette clusters remained unaffected. This was accompanied by transiently increased expression of the neural progenitor TF *FoxA2*, decreased expression of the neural differentiation products *Tubb3* and *Map2* (Fig. 3h-i), and reduced TUBB3/TUJ1 immunostaining compared to control cells at D5 (Fig. 3e). By D10, however, the abundance of axon bundles and TUJ1 immunostaining in GLI1 OE cells were statistically indistinguishable from those of control cells (Fig. 3f-g), and the expression of neural progenitor and differentiation markers had normalized to control levels (Fig. 3h-i). These results indicated that transient GLI1 OE caused pan-neuronal differentiation delay, but did not alter differentiation potential, similar to its effect in cardiac progenitors. Together, these findings are consistent with the ability of Hh GLI^A TFs to transiently delay differentiation across germ layers.

GLI1 expression in neuronal progenitors maintained progenitor gene expression at the expense of differentiation gene expression, suggesting an inverse relationship

between Hh signaling activation and ectodermal differentiation. Hh signaling hyperactivation has been implicated as a cause of the neuronal cancer medulloblastoma, which has been modelled in the adult mouse by *Ptch1* heterozygosity (*Ptch1*$^{+/-}$)[39]. We examined whether *Ptch1*-dependent gene expression correlated with ectodermal differentiation stage gene expression. We identified stage-specific gene expression programs in the ectoderm, performing differential expression analysis between ectodermal progenitors and differentiated ectoderm tissues from available datasets[43]. We then examined whether there was a correlation between stage-specific gene expression in the ectoderm (ectoderm progenitor vs. differentiated ectoderm fold change) and *Ptch1*-deoendent gene expression in the *Ptch1*$^{+/-}$ adult mouse medulla[56] (*Ptch1*$^{+/-}$ vs. *Ptch1*$^{+/+}$ fold change). We observed a strong, negative correlation between expression changes due to *Ptch1* heterozygosity and expression changes occurring during ectoderm differentiation (Fig. 3j). Furthermore, when compared to the distribution of genes differentially expressed between ectoderm progenitors and differentiated ectoderm, *Ptch1*$^{+/-}$-activated genes were over-represented among genes highly expressed in the progenitor-specific state and *Ptch1*$^{+/-}$-repressed genes were over-represented among genes highly expressed in the differentiated-specific state (Fig. 2k). Taken together, our observations in cardiac and neuronal contexts suggest that Hh signaling activation promotes the activation and maintenance of progenitor-specific gene expression programs while preventing differentiation-specific gene expression programs in cells of diverse developmental origins and in a *Hh*-dependent adult cancer model.

We hypothesized that Hh signaling globally promotes progenitor maintenance through direct GLI^{A} activation of a progenitor-specific regulatory network. Using ATAC-

seq[57], we identified candidate GLI1-dependent regulatory regions by comparing accessible chromatin regions in doxycycline-induced GLI1 OE cardiac progenitors to untreated control cells. We found 8,001 newly accessible regions upon GLI1 OE in cardiac progenitors (Fig. 4a). We reasoned that if GLI1 OE results in the activation of a progenitor-specific gene regulatory network, then progenitor-specific TF motifs would be enriched within GLI1 OE-specific accessible regulatory regions controlling this network. *De novo* motif analysis of GLI1 OE-specific accessible chromatin regions revealed strong enrichment of GLI and FOX motifs (Extended Data Fig 7a), suggestive of induced mesoderm progenitor TF activity. Interestingly, motif enrichment was also observed for ZFX, REST and HIC1, three TFs known to cooperatively activate transcription with GLI TFs in neural progenitors and to propagate Hh-activated medulloblastoma[58-61], suggesting that GLI^A TFs may activate progenitor gene expression in coordination with a common set of co-factors in both cardiac and neural contexts. In contrast, accessible regions that were lost upon GLI1 OE were enriched for motifs of TFs that drive mesodermal differentiation, including TAL1 (blood) and NKX2-5 (cardiac and head musculature).

Numerous studies have demonstrated that Hh signaling ensures the survival of stem cell populations through proliferation control[10, 34-37, 62-93], however, the mechanism by which GLI^A TFs control proliferation remains unclear. While we observed upregulation of cell cycle regulators upon GLI1 OE, the most highly dysregulated genes were not cell cycle genes but instead included cardiac progenitor TFs, and were associated with developmental and differentiation GO terms (Fig. 2i). Interestingly, we did not observe appreciable chromatin reorganization at the promoters of cell cycle regulators *Myc*, *Mycn,*

Cdk6 and *Ccnd1* (Extended Data Fig. 7c-f), bound by GLI TFs in other contexts[94-98], suggesting that GLI^A does not maintain progenitor status through direct regulation of this class of genes in cardiac progenitors.

We further examined the genomic distribution of accessible regions specific to GLI1 OE progenitors. Chromatin at the promoters of direct GLI^A targets, such as *Gli1*, *Foxf1 and Ptch1*, were rendered more accessible upon GLI1 OE (Extended Data Fig. 7g-i). However, we observed that the majority of chromatin reorganization occurred at regions distal to transcriptional start sites, which are putative GLI-dependent *cis*-regulatory elements (CREs) (Extended Data Fig. 7b). Of all 73,471 distal accessible regions in GLI1 OE or control cells, we identified 18,305 (25%) putative CREs that contained GLI binding motifs[95, 99]. Of these, 1,162 (6%) were located within 150kb of *Shh*-dependent pSHF genes. We next compared cardiac progenitor and differentiated cardiomyocyte ATAC profiles *in vitro* and *in vivo*. We analyzed the global concordance of ATAC-seq signal intensity between GLI1 OE and control *in vitro* accessible regions with E10.5 pSHF *in vivo* progenitor accessible regions. The accessibility correlation between GLI1 OE accessible regions and pSHF regions was higher (r = 0.71) than that between control accessible regions and pSHF regions (r = 0.61; Fig. 4b, gold box). Consistent with this observation, distal CREs near known Hh-dependent targets gained accessibility upon GLI1 OE *in vitro*, acquiring the accessibility profile of the pSHF (Extended Data Fig. 7j, grey boxes, region upstream of the Hh target, *Ptch1*). These observations indicate that GLI^A TFs promote cardiac progenitor-specific chromatin accessibility at distal CREs, providing a genomic mechanistic for maintaining progenitor-specific TF expression of Hh target genes.

We hypothesized that the removal of cells from active Hh signaling, permitting a progenitor-to-differentiation regulatory network transition, is mechanistically enacted by a GLI^A to GLI^R switch at regulatory elements near progenitor-specific genes. This model predicts that the activity of progenitor-specific CREs is dictated by the local abundance of GLI^A vs GLI^R TFs. We previously identified a GLI-bound distal CRE upstream of the SHF Hh target gene *Foxf1*[26]. This enhancer drives pSHF-specific reporter expression and is silenced in the HT *in vivo*, representing a progenitor-active CRE and candidate molecular target for a GLI^A to GLI^R switch. Chromatin at the *Foxf1* CRE became more accessible upon GLI1 OE *in vitro*, similar to the pSHF *in vivo* (Fig. 4c), suggesting that GLI1 OE may lead to increased enhancer activity. This CRE contains three binding motifs for GLI, three binding motifs for the cardiogenic TF TBX5[26], and is bound by both GLI and TBX5 in the pSHF *in-vivo* [95, 100]. We examined the ability of GLI TFs to modulate the activation of this enhancer, using a luciferase transcriptional reporter assay. TBX5 activated reporter expression from the wild type *Foxf1* CRE *in vitro* (Fig. 4d). Mutation of all three TBX5 binding sites abrogated CRE activation. Co-transfection of GLI1 with TBX5 dramatically enhanced transcriptional activation from the wild type *Foxf1* CRE. Mutation of the TBX5 or GLI binding sites moderated this activation. Co-transfection of $GLI3^R$ with TBX5 silenced TBX5-dependent transcriptional activation (Fig. 4d). These results established that cellular GLI^A versus GLI^R TF abundance was a dominant predictor of the activity of this *Foxf1* progenitor CRE *in vitro*.

A GLI^A to GLI^R transition is experienced by cardiac progenitors as they migrate from the pSHF into the HT [24-26]. We hypothesized that this transition established a functional high-to-low CRE activity switch to localize progenitor-specific CRE activity *in*

vivo. We tested this hypothesis by investigating whether GLI binding sites were required for the progenitor *CRE* at *Foxf1* to switch from active in cardiac progenitors to silenced in the differentiated heart. The wild type *Foxf1* CRE demonstrated SHF-specific activity *in vivo*[26]. In contrast, the *Foxf1* CRE harboring mutated GLI binding sites demonstrated ectopic reporter expression in the HT (5/5 GLI binding site mutant embryos with HT expression, Fig. 4e; gold box and Extended Data Fig. 8a-b). This observation indicating that GLI binding sites were required to restrict activation of this enhancer to pSHF progenitors.

We hypothesized that the GLI^A to GLI^R switch mechanism determined the location of differentiation of pSHF cardiac progenitors *in vivo*. We evaluated myocardial differentiation in $Shh^{-/-}$ embryos, which lack the pulmonary to pSHF Hh activating signal, and therefore GLI^A activity, in the pSHF[25]. While wild type littermate control embryos demonstrated expression of sarcomeric myosin (MF20) only in the differentiating HT, ectopic expression of sarcomeric myosin was observed in the pSHF of $Shh^{-/-}$ mice at E10.5, in concert with the absence of mesenchymal progenitor cells that normally migrate into the heart from the pSHF (Fig. 4f, yellow arrowhead). By E14.5, $Shh^{-/-}$ embryos demonstrated CHD (atrioventricular septal defects (AVSDs)), consistent with previous reports[101-104]. We next hypothesized that GLI-dependent differentiation timing in the SHF was exerted through the GLI TF switch mechanism. We tested this hypothesis by overriding GLI^A activity using SHF-specific GLI^R overexpression. We induced indelible expression of $GLI3^R$ from the *Cre*-dependent $ROSA26^{Gli3T\text{-}Flag\ c/c}$ allele[95] in the pSHF using the tamoxifen-inducible $Osr1^{eGFPCre\text{-}ERt2}$ allele[105], expressed in the pSHF but not the heart. Indelible expression of $GLI3^R$ in $Osr1^{eGFPCre\text{-}ERt2/+}$; $ROSA26^{Gli3T\text{-}Flag\ c/+}$ mice, administered

tamoxifen daily from E7.5 to E9.5, caused precocious cardiomyocyte differentiation in the pSHF, evidenced by the appearance of sarcomeric myosin (MF20) expression, and absence of mesenchymal progenitor cells migrating into the HT, compared to *ROSA26*$^{Gli3T\text{-}Flag\ c/+}$ littermate controls at E10.5 (Fig. 4f). Mutant embryos, but not littermate controls, demonstrated AVSDs at E14.5. Together, these findings indicated that Hh signaling maintained pSHF progenitor status by promoting SHF GLI^{A} TF predominance, permitting the accretion of cardiac progenitors to the HT where differentiation subsequently commences. Thus, premature deployment of GLI^{R} TF predominance, directly or by abrogation of Hh signaling, causes premature cardiac progenitor differentiation and CHD.

The results presented here indicate that GLI-dependent CREs comprise a molecular switch at progenitor-specific genes, providing a model for translating spatially distributed GLI^{A}/GLI^{R} TF ratios into a differentiation timing mechanism. This model suggests that in some contexts, differentiation can be delayed by Hh-dependent maintenance of progenitor-specific gene expression. This work implies that a release of differentiation delay requires that cells transition from active Hh signaling environments with GLI^{A} predominance to inactive Hh signaling environments with GLI^{R} predominance, implicating GLI TF transition as a biphasic switch that determines progenitor differentiation timing (Fig. 4g). This GLI^{A} to GLI^{R} transition could be mediated either by migration of cells away from the source of activating Hh ligand or by termination of ligand production. Here, we provide evidence for the former mechanism in the embryonic pSHF, linking the spatial distribution of signal-dependent GLI TFs to the differentiation timing of a progenitor population.

Hh signaling has been implicated in maintenance of stem cell niches for repair and regeneration of several adult tissues. Hh signaling functions to maintain or expand quiescent stem cell populations in many organs, including the regenerating hair follicle[3,106], intestine[107-108], bladder epithelial cells[109], adult lung epithelium[110], skin[111], prostate[38] and brain[17, 112]. Additionally, Hh signaling activation of progenitor proliferation has been nominated as a common mechanism linking developmental mechanisms to tumorigenesis[2, 4-8, ,58, 113-124]. Our analysis of gene expression in medulloblastoma (Fig. 3j,k) supports the idea that Hh signaling drives cancer progression through the activation or maintenance of a progenitor-specific TF network that maintains the progenitor state at the expense of a differentiation program. We therefore postulate that some previously observed effects linking active Hh signaling to increased proliferation may be secondary to the maintenance of a progenitor state within inherent proliferative capacity.

GLI TFs pattern the embryonic ventral neural tube by activating repressive TFs that prevent the acquisition of alternate fates[49-53, 125-128]. Here, we have linked a disruption of GLI^A / GLI^R TF transition to precocious differentiation and structural heart defects (Fig. 4f). While we have not examined the developing CNS *in vivo*, previous work found that indelible *Gli1* expression in the neural tube prevented neuronal differentiation[58]. This, combined with our parallel observations from cardiac and neural models of development, raise the possibility that GLI activity is widely employed as a molecular switch for controlling differentiation timing. Our results are not inconsistent with previous studies demonstrating a role for GLI TFs in neuronal subtype specification; instead we suggest that neural specification may be tied to differentiation timing. This study opens new opportunities to investigate potential mechanistic links between the well-documented

effects of Hh gradient thresholds[12, 128-130] and signaling duration[131-134] on cell subtype specification and the novel role of GLI^A TFs in controlling differentiation timing. Important unanswered questions include: Do GLI TF-dependent progenitor transcription factor networks function via common mechanisms to maintain progenitor status in different lineages? How is Hh-mediated control of differentiation timing coupled to the cell cycle machinery? To what extent can the power of GLI^A to promote progenitor status and proliferation be used to enhance regenerative potential[98, 135]? Does Hh signaling interaction with the Wnt signaling pathway contribute to differentiation timing control[15, 136-137]? Future efforts to address these questions may lead to improved understanding of organogenesis and potentially to novel therapeutic approaches for diseases involving aberrant Hh activity, including congenital heart defects, medulloblastoma and basal cell carcinoma. We posit a unifying role for Hh signaling in the maintenance of progenitor populations and inhibition of differentiation across multiple tissue types during development, adult tissue homeostasis and disease.

References

1. Morrison SJ, Spradling AC. Stem cells and niches: mechanisms that promote stem cell maintenance throughout life. *Cell* **132**, 598-611 (2008).

2. Briscoe J, Thérond PP. The mechanisms of Hedgehog signalling and its roles in development and disease. *Nat Rev Mol Cell Biol.* **14**, 416-29 (2013).

3. Hsu YC, Li L, Fuchs E. Transit-amplifying cells orchestrate stem cell activity and tissue regeneration. *Cell* **157**, 935-49 (2014).

4. Briscoe J, Small S. Morphogen rules: design principles of gradient-mediated embryo patterning. *Development* **142**, 3996-4009 (2015).

5. McCabe JM, Leahy DJ. Smoothened goes molecular: new pieces in the hedgehog signaling puzzle. *J Biol Chem.* **290**, 3500-7 (2015).

6. Singh BN, Koyano-Nakagawa N, Donaldson A, Weaver CV, Garry MG, Garry DJ. Hedgehog Signaling during Appendage Development and Regeneration. *Genes (Basel)* **6**, 417-35 (2015).

7. Belgacem YH, Hamilton AM, Shim S, Spencer KA, Borodinsky LN. The Many Hats of Sonic Hedgehog Signaling in Nervous System Development and Disease. *J Dev Biol*. **4**, 35 (2016).

8. Lee RT, Zhao Z, Ingham PW. Hedgehog signalling. *Development* **143**, 367-72 (2016).

9. Petrov K, Wierbowski BM, Salic A. Sending and Receiving Hedgehog Signals. *Annu Rev Cell Dev Biol.* **33**,145-168 (2017).

10. Wechsler-Reya RJ, Scott MP. Control of neuronal precursor proliferation in the cerebellum by Sonic Hedgehog. *Neuron* **22**, 103-14 (1999).

11. Aza-Blanc P, Lin HY, Ruiz i Altaba A, Kornberg TB. Expression of the vertebrate Gli proteins in Drosophila reveals a distribution of activator and repressor activities. *Development* **127**, 4293-301 (2000).

12. Müller B, Basler K. The repressor and activator forms of Cubitus interruptus control Hedgehog target genes through common generic gli-binding sites. *Development* **127**, 2999-3007 (2000).

13. Wang B, Fallon JF, Beachy PA. Hedgehog-regulated processing of Gli3 produces an anterior/posterior repressor gradient in the developing vertebrate limb. *Cell* **100**, 423-34 (2000).

14. Lai K, Kaspar BK, Gage FH, Schaffer DV. Sonic hedgehog regulates adult neural progenitor proliferation in vitro and in vivo. *Nat Neurosci.* **6**, 21-7 (2003).

15. Beachy PA, Karhadkar SS, Berman DM. Tissue repair and stem cell renewal in carcinogenesis. *Nature* **432**, 324-31 (2004).

16. Hooper JE, Scott MP. Communicating with Hedgehogs. *Nat Rev Mol Cell Biol.* **6**, 306-17 (2004).

17. Ahn S, Joyner AL. In vivo analysis of quiescent adult neural stem cells responding to Sonic hedgehog. *Nature* **437**, 894-7 (2005).

18. Ingham PW, Placzek M. Orchestrating ontogenesis: variations on a theme by sonic hedgehog. *Nat Rev Genet.* **7**, 841-50 (2006).

19. Pan Y, Bai CB, Joyner AL, Wang B. Sonic hedgehog signaling regulates Gli2 transcriptional activity by suppressing its processing and degradation. *Mol Cell Biol.* **26**, 3365-77 (2006).

20. Mandal L, Martinez-Agosto JA, Evans CJ, Hartenstein V, Banerjee U. A Hedgehog- and Antennapedia-dependent niche maintains Drosophila haematopoietic precursors. *Nature* **446**, 320-4 (2007).

21. Ruiz i Altaba A, Mas C, Stecca B. The Gli code: an information nexus regulating cell fate, stemness and cancer. *Trends Cell Biol.* **17**, 438-47 (2007).

22. Hui CC, Angers S. Gli proteins in development and disease. *Annu Rev Cell Dev Biol.* **27**, 513-37 (2011).

23. Ingham PW, Nakano Y, Seger C. Mechanisms and functions of Hedgehog signaling across the metazoa. *Nat Rev Genet.* **12**, 393-406 (2011).

24. Goddeeris, M. M. *et al.* Intracardiac septation requires hedgehog-dependent cellular contributions from outside the heart. *Development* **135,** 1887–1895 (2008).

25. Hoffmann, A. D., Peterson, M. A., Friedland-Little, J. M., Anderson, S. A. & Moskowitz, I. P. sonic hedgehog is required in pulmonary endoderm for atrial septation. *Development* **136**, 1761–1770 (2009).

26. Hoffmann, A. D. *et al.* PLOS Genetics: Foxf Genes Integrate Tbx5 and Hedgehog Pathways in the Second Heart Field for Cardiac Septation. *journals.plos.org* 10, e1004604 (2014).

27. Kelly RG. The second heart field. *Curr Top Dev Biol* **100**, 33-65 (2012).

28. Peterson RS, Lim L, Ye H, Zhou H, Overdier DG, Costa RH. The winged helix transcriptional activator HFH-8 is expressed in the mesoderm of the primitive streak stage of mouse embryos and its cellular derivatives. *Mech Dev.* **69**, 53-69 (1997).

29. Mahlapuu M, Ormestad M, Enerbäck S, Carlsson P. The forkhead transcription factor Foxf1 is required for differentiation of extra-embryonic and lateral plate mesoderm. *Development* **128**, 155-66 (2001).

30. Wang Q, Lan Y, Cho ES, Maltby KM, Jiang R. Odd-skipped related 1 (Odd 1) is an essential regulator of heart and urogenital development. *Dev Biol.* **288**, 582-94 (2005).

31. Goss AM, Tian Y, Tsukiyama T, Cohen ED, Zhou D, Lu MM, Yamaguchi TP, Morrisey EE. Wnt2/2b and beta-catenin signaling are necessary and sufficient to specify lung progenitors in the foregut. *Dev Cell* **17**, 290-8 (2009).

32. Harris-Johnson KS, Domyan ET, Vezina CM, Sun X. beta-Catenin promotes respiratory progenitor identity in mouse foregut. *Proc Natl Acad Sci U S A.* **106**, 16287-92 (2009).

33. Tao G, Levay AK, Gridley T, Lincoln J. Mmp15 is a direct target of Snai1 during endothelial to mesenchymal transformation and endocardial cushion development. *Dev Biol.* **359**, 209-21 (2011).

34. Zhang Y, Kalderon D. Regulation of cell proliferation and patterning in Drosophila oogenesis by Hedgehog signaling. *Development* **127**, 2165-76 (2000).

35. Bhardwaj G, Murdoch B, Wu D, Baker DP, Williams KP, Chadwick K, Ling LE, Karanu FN, Bhatia M. Sonic hedgehog induces the proliferation of primitive human hematopoietic cells via BMP regulation. *Nat Immunol.* **2**, 172-80 (2001).

36. Zhang Y, Kalderon D. Hedgehog acts as a somatic stem cell factor in the Drosophila ovary. *Nature* **410**, 599-604 (2001).

37. Machold R, Hayashi S, Rutlin M, Muzumdar MD, Nery S, Corbin JG, Gritli-Linde A, Dellovade T, Porter JA, Rubin LL, Dudek H, McMahon AP, Fishell G. Sonic hedgehog is required for progenitor cell maintenance in telencephalic stem cell niches. *Neuron* **39**, 937-50 (2003).

38. Karhadkar SS, Bova GS, Abdallah N, Dhara S, Gardner D, Maitra A, Isaacs JT, Berman DM, Beachy PA. Hedgehog signalling in prostate regeneration, neoplasia and metastasis. *Nature* **431**, 707-12 (2004).

39. Goodrich LV, Milenković L, Higgins KM, Scott MP. Altered neural cell fates and medulloblastoma in mouse patched mutants. *Science* **277**, 1109-13 (1997).

40. Lee J, Platt KA, Censullo P, Ruiz i Altaba A. Gli1 is a target of Sonic hedgehog that induces ventral neural tube development. *Development* **124**, 2537-52 (1997).

41. Büscher D, Rüther U. Expression profile of Gli family members and Shh in normal and mutant mouse limb development. *Dev Dyn.* **211**, 88-96 (1998).

42. Dai P, Akimaru H, Tanaka Y, Maekawa T, Nakafuku M, Ishii S. Sonic Hedgehog-induced activation of the Gli1 promoter is mediated by GLI3. *J Biol Chem*. **274**, 8143-52 (1999).

43. ENCODE Project Consortium. An integrated encyclopedia of DNA elements in the human genome. *Nature* **489**, 57-74 (2012).

44. Kattman SJ, Witty AD, Gagliardi M, Dubois NC, Niapour M, Hotta A, Ellis J, Keller G. Stage-specific optimization of activin/nodal and BMP signaling promotes cardiac differentiation of mouse and human pluripotent stem cell lines. *Cell Stem Cell* **8**, 228-40 (2011).

45. Hynes M, Stone DM, Dowd M, Pitts-Meek S, Goddard A, Gurney A, Rosenthal A. Control of cell pattern in the neural tube by the zinc finger transcription factor and oncogene Gli-1. *Neuron* **19**, 15-26 (1997).

46. Sasaki H, Hui C, Nakafuku M, Kondoh H. A binding site for Gli proteins is essential for HNF-3beta floor plate enhancer activity in transgenics and can respond to Shh in vitro. *Development* **124**, 1313-22 (1997).

47. Ruiz i Altaba A. Combinatorial Gli gene function in floor plate and neuronal inductions by Sonic hedgehog. *Development* **125**, 2203-12 (1998).

48. Ruiz i Altaba A. Gli proteins encode context-dependent positive and negative functions: implications for development and disease. *Development* **126**, 3205-16 (1999).

49. Ericson, J., Morton, S., Kawakami, A., Roelink, H. & Jessell, T. M. Two critical periods of Sonic Hedgehog signaling required for the specification of motor neuron identity. *Cell* **87**, 661-673 (1996).

50. Briscoe, J., Pierani, A., Jessell, T. M. & Ericson, J. A homeodomain protein code specifies progenitor cell identity and neuronal fate in the ventral neural tube. *Cell* **101**, 435-445 (2000).

51. Dessaud, E., McMahon, A. P. & Briscoe, J. Pattern formation in the vertebrate neural tube: a sonic hedgehog morphogen-regulated transcriptional network. *Development* **135**, 2489-2503 (2008).

52. Sasai N, Kutejova E, Briscoe J. Integration of signals along orthogonal axes of the vertebrate neural tube controls progenitor competence and increases cell diversity. *PLoS Biol.* **12**, e1001907 (2014).

53. Kutejova E, Sasai N, Shah A, Gouti M, Briscoe J. Neural Progenitors Adopt Specific Identities by Directly Repressing All Alternative Progenitor Transcriptional Programs. *Dev Cell* **36**, 639-53 (2016).

54. Ying, Q.-L. & Smith, A. G. Defined conditions for neural commitment and differentiation. *Methods in enzymology* **365**, 327-341 (2003).

55. Ferreira, A. & Caceres, A. Expression of the Class III β-tubulin isotype in developing neurons in culture. *Journal of neuroscience research* **32**, 516-529 (1992).

56. Grausam KB, Dooyema SDR, Bihannic L, Premathilake H, Morrissy AS, Forget A, Schaefer AM, Gundelach JH, Macura S, Maher DM, Wang X, Heglin AH, Ge X, Zeng E, Puget S, Chandrasekar I, Surendran K, Bram RJ, Schüller U, Talyor MD, Ayrault O, Zhao H. ATOH1 Promotes Leptomeningeal Dissemination and Metastasis of Sonic Hedgehog Subgroup Medulloblastomas. *Cancer Res.* **77**, 3766-3777 (2017).

57. Buenrostro JD, Giresi PG, Zaba LC, Chang HY, Greenleaf WJ. Transposition of native chromatin for fast and sensitive epigenomic profiling of open chromatin, DNA-binding proteins and nucleosome position. *Nat Methods* **10**, 1213-8 (2013).

58. Palmer CJ, Galan-Caridad JM, Weisberg SP, Lei L, Esquilin JM, Croft GF, Wainwright B, Canoll P, Owens DM, Reizis B. Zfx facilitates tumorigenesis caused by activation of the Hedgehog pathway. *Cancer Res.* **74**, 5914-24 (2014).

59. Briggs KJ, Corcoran-Schwartz IM, Zhang W, Harcke T, Devereux WL, Baylin SB, Eberhart CG, Watkins DN. Cooperation between the Hic1 and Ptch1 tumor suppressors in medulloblastoma. *Genes Dev*. **22**, 770-85 (2008).

60. Ballas N, Grunseich C, Lu DD, Speh JC, Mandel G. REST and its corepressors mediate plasticity of neuronal gene chromatin throughout neurogenesis. *Cell* **121**, 645-657 (2005).

61. Shi X, Wang Q, Gu J, Xuan Z, Wu JI. SMARCA4/Brg1 coordinates genetic and epigenetic networks underlying Shh-type medulloblastoma development. *Oncogene* **35**, 5746-5758 (2016).

62. Fan H, Khavari PA. Sonic hedgehog opposes epithelial cell cycle arrest. *J Cell Biol.* **147**, 71-6 (1999).

63. Rowitch DH, S-Jacques B, Lee SM, Flax JD, Snyder EY, McMahon AP. Sonic hedgehog regulates proliferation and inhibits differentiation of CNS precursor cells. *J Neurosci*. **19**, 8954-65 (1999).

64. Kenney AM, Rowitch DH. Sonic hedgehog promotes G(1) cyclin expression and sustained cell cycle progression in mammalian neuronal precursors. *Mol Cell Biol.* **20**, 9055-67 (2000).

65. Barnes EA, Kong M, Ollendorff V, Donoghue DJ. Patched1 interacts with cyclin B1 to regulate cell cycle progression. *EMBO J.* **20**, 2214-23 (2001).

66. Dahmane N, Sánchez P, Gitton Y, Palma V, Sun T, Beyna M, Weiner H, Ruiz i Altaba A. The Sonic Hedgehog-Gli pathway regulates dorsal brain growth and tumorigenesis. *Development* **128**, 5201-12 (2001).

67. Ruiz i Altaba A, Palma V, Dahmane N. Hedgehog-Gli signalling and the growth of the brain. *Nat Rev Neurosci.* **3**, 24-33 (2002).

68. Mill P, Mo R, Fu H, Grachtchouk M, Kim PC, Dlugosz AA, Hui CC. Sonic hedgehog-dependent activation of Gli2 is essential for embryonic hair follicle development. *Genes Dev.* **17**, 282-94 (2003).

69. Fu M, Lui VC, Sham MH, Pachnis V, Tam PK. Sonic hedgehog regulates the proliferation, differentiation, and migration of enteric neural crest cells in gut. *J Cell Biol.* **166**, 673-84 (2004).

70. Palma V, Ruiz i Altaba A. Hedgehog-GLI signaling regulates the behavior of cells with stem cell properties in the developing neocortex. *Development* **131**, 337-45 (2004).

71. Romer JT, Kimura H, Magdaleno S, Sasai K, Fuller C, Baines H, Connelly M, Stewart CF, Gould S, Rubin LL, Curran T. Suppression of the Shh pathway using a small molecule inhibitor eliminates medulloblastoma in Ptc1(+/-)p53(-/-) mice. *Cancer Cell* **6**, 229-40 (2004).

72. Sanchez P, Hernández AM, Stecca B, Kahler AJ, DeGueme AM, Barrett A, Beyna M, Datta MW, Datta S, Ruiz i Altaba A. Inhibition of prostate cancer proliferation by interference with SONIC HEDGEHOG-GLI1 signaling. *Proc Natl Acad Sci U S A.* **101**, 12561-6 (2004).

73. Mill P, Mo R, Hu MC, Dagnino L, Rosenblum ND, Hui CC. Shh controls epithelial proliferation via independent pathways that converge on N-Myc. *Dev Cell* **9**, 293-303 (2005).

74. Bénazéraf B, Chen Q, Peco E, Lobjois V, Médevielle F, Ducommun B, Pituello F. Identification of an unexpected link between the Shh pathway and a G2/M regulator, the phosphatase CDC25B. *Dev Biol.* **294**, 133-47 (2006).

75. Cayuso J, Ulloa F, Cox B, Briscoe J, Martí E. The Sonic hedgehog pathway independently controls the patterning, proliferation and survival of neuroepithelial cells by regulating Gli activity. *Development* **133**, 517-28 (2006).

76. Trowbridge JJ, Scott MP, Bhatia M. Hedgehog modulates cell cycle regulators in stem cells to control hematopoietic regeneration. *Proc Natl Acad Sci U S A.* **103**, 14134-9 (2006).

77. Heo JS, Lee MY, Han HJ. Sonic hedgehog stimulates mouse embryonic stem cell proliferation by cooperation of Ca2+/protein kinase C and epidermal growth factor receptor as well as Gli1 activation. *Stem Cells* **25**, 3069-80 (2007).

78. Ou CY, Wang CH, Jiang J, Chien CT. Suppression of Hedgehog signaling by Cul3 ligases in proliferation control of retinal precursors. *Dev Biol.* **308**,106-19 (2007).

79. Dierks C, Beigi R, Guo GR, Zirlik K, Stegert MR, Manley P, Trussell C, Schmitt-Graeff A, Landwerlin K, Veelken H, Warmuth M. Expansion of Bcr-Abl-positive leukemic stem cells is dependent on Hedgehog pathway activation. *Cancer Cell* **14**, 238-49 (2008).

80. Laner-Plamberger S, Kaser A, Paulischta M, Hauser-Kronberger C, Eichberger T, Frischauf AM. Cooperation between GLI and JUN enhances transcription of JUN and selected GLI target genes. *Oncogene* **28**, 1639-51 (2009).

81. Li F, Duman-Scheel M, Yang D, Du W, Zhang J, Zhao C, Qin L, Xin S. Sonic hedgehog signaling induces vascular smooth muscle cell proliferation via induction of the G1 cyclin-retinoblastoma axis. *Arterioscler Thromb Vasc Biol.* **30**, 1787-94 (2010).

82. Merchant A, Joseph G, Wang Q, Brennan S, Matsui W. Gli1 regulates the proliferation and differentiation of HSCs and myeloid progenitors. *Blood* **115**, 2391-6 (2010).

83. Colvin Wanshura LE, Galvin KE, Ye H, Fernandez-Zapico ME, Wetmore C. Sequential activation of Snail1 and N-Myc modulates sonic hedgehog-induced transformation of neural cells. *Cancer Res.* **71**, 5336-45 (2011).

84. Feijóo CG, Oñate MG, Milla LA, Palma VA. Sonic hedgehog (Shh)-Gli signaling controls neural progenitor cell division in the developing tectum in zebrafish. *Eur J Neurosci.* **33**, 589-98 (2011).

85. Plaisant M, Giorgetti-Peraldi S, Gabrielson M, Loubat A, Dani C, Peraldi P. Inhibition of hedgehog signaling decreases proliferation and clonogenicity of human mesenchymal stem cells. *PLoS One* **6**, e16798 (2011).

86. Wang H, Ge G, Uchida Y, Luu B, Ahn S. Gli3 is required for maintenance and fate specification of cortical progenitors. *J Neurosci.* **31**, 6440-8 (2011).

87. Milla LA, Arros A, Espinoza N, Remke M, Kool M, Taylor MD, Pfister SM, Wainwright BJ, Palma V. Neogenin1 is a Sonic Hedgehog target in medulloblastoma and is necessary for cell cycle progression. *Int J Cancer* **134**, 21-31 (2014).

88. Zinke J, Schneider FT, Harter PN, Thom S, Ziegler N, Toftgård R, Plate KH, Liebner S. β-Catenin-Gli1 interaction regulates proliferation and tumor growth in medulloblastoma. Mol Cancer. 2015 Feb 3;14:17. Srivastava RK, Kaylani SZ, Edrees N, Li C, Talwelkar SS, Xu J, Palle K, Pressey JG, Athar M. GLI inhibitor GANT-61 diminishes embryonal and alveolar rhabdomyosarcoma growth by inhibiting Shh/AKT-mTOR axis. *Oncotarget* **5**, 12151-65 (2014).

89. Jafari SM, Joshaghani HR, Panjehpour M, Aghaei M, Zargar Balajam N. Apoptosis and cell cycle regulatory effects of adenosine by modulation of GLI-1 and ERK1/2 pathways in CD44(+) and CD24(-) breast cancer stem cells. *Cell Prolif.* doi: 10.1111/cpr.12345 (2017).

90. Lin Z, Sheng H, You C, Cai M, Zhang Y, Yu LS, Yu X, Lin J, Zhang N. Inhibition of the CyclinD1 promoter in response to sonic hedgehog signaling pathway transduction is mediated by Gli1. E*xp Ther Med.* **13**, 307-314 (2017).

91. Miele E, Po A, Begalli F, Antonucci L, Mastronuzzi A, Marras CE, Carai A, Cucchi D, Abballe L, Besharat ZM, Catanzaro G, Infante P, Di Marcotullio L, Canettieri G, De Smaele E, Screpanti I, Locatelli F, Ferretti E. β-arrestin1-mediated acetylation of

Gli1 regulates Hedgehog/Gli signaling and modulates self-renewal of SHH medulloblastoma cancer stem cells. *BMC Cancer* **17**, 488 (2017).

92. Wang D, Hu G, Du Y, Zhang C, Lu Q, Lv N, Luo S. Aberrant activation of hedgehog signaling promotes cell proliferation via the transcriptional activation of forkhead Box M1 in colorectal cancer cells. *J Exp Clin Cancer Res.* **36**, 23 (2017).

93. Nanta R, Shrivastava A, Sharma J, Shankar S, Srivastava RK. Inhibition of sonic hedgehog and PI3K/Akt/mTOR pathways cooperate in suppressing survival, self-renewal and tumorigenic potential of glioblastoma-initiating cells. *Mol Cell Biochem.* doi: 10.1007/s11010-018-3448-z (2018).

94. Hu MC, Mo R, Bhella S, Wilson CW, Chuang PT, Hui CC, Rosenblum ND. GLI3-dependent transcriptional repression of Gli1, Gli2 and kidney patterning genes disrupts renal morphogenesis. *Development* **133**, 569-78 (2006).

95. Vokes SA, Ji H, Wong WH, McMahon AP. A genome-scale analysis of the cis-regulatory circuitry underlying sonic hedgehog-mediated patterning of the mammalian limb. *Genes Dev*. **22**, 2651-63 (2008).

96. Milla LA, Cortés CR, Hodar C, Oñate MG, Cambiazo V, Burgess SM, Palma V. Yeast-based assay identifies novel Shh/Gli target genes in vertebrate development. *BMC Genomics* **13**, 2 (2012).

97. Hasenpusch-Theil K, West S, Kelman A, Kozic Z, Horrocks S, McMahon AP, Price DJ, Mason JO, Theil T. Gli3 controls the onset of cortical neurogenesis by regulating the radial glial cell cycle through Cdk6 expression. *Development* **145** (2018).

98. Singh BN, Koyano-Nakagawa N, Gong W, Moskowitz IP, Weaver CV, Braunlin E, Das S, van Berlo JH, Garry MG, Garry DJ. A conserved HH-Gli1-Mycn network regulates heart regeneration from newt to human. *Nat Commun*. **9**, 4237 (2018).

99. Hallikas O, Palin K, Sinjushina N, Rautiainen R, Partanen J, Ukkonen E, Taipale J. Genome-wide prediction of mammalian enhancers based on analysis of transcription-factor binding affinity. *Cell* **124**, 47-59 (2006).

100. Luna-Zurita L, Stirnimann CU, Glatt S, Kaynak BL, Thomas S, Baudin F, Samee MA, He D, Small EM, Mileikovsky M, Nagy A, Holloway AK, Pollard KS, Müller CW, Bruneau BG. Complex Interdependence Regulates Heterotypic Transcription Factor Distribution and Coordinates Cardiogenesis. *Cell* **164**, 999-1014 (2016).

101. Izraeli S, Lowe LA, Bertness VL, Good DJ, Dorward DW, Kirsch IR, Kuehn MR. The SIL gene is required for mouse embryonic axial development and left-right specification. *Nature* **399**, 691-4 (1999).

102. Meyers EN, Martin GR. Differences in left-right axis pathways in mouse and chick: functions of FGF8 and SHH. *Science* **285**, 403-6 (1999).

103. Tsukui T, Capdevila J, Tamura K, Ruiz-Lozano P, Rodriguez-Esteban C, Yonei-Tamura S, Magallón J, Chandraratna RA, Chien K, Blumberg B, Evans RM, Belmonte JC. Multiple left-right asymmetry defects in Shh(-/-) mutant mice unveil a convergence of the shh and retinoic acid pathways in the control of Lefty-1. *Proc Natl Acad Sci U S A*. **96**, 11376-81 (1999).

104. Kim PC, Mo R, Hui Cc C. Murine models of VACTERL syndrome: Role of sonic hedgehog signaling pathway. *J Pediatr Surg.* **36**, 381-4 (2001).

105. Mugford, J. W., Sipilae, P., McMahon, J. A. & McMahon, A. P. Osr1 expression demarcates a multi-potent population of intermediate mesoderm that undergoes progressive restriction to an Osr1-dependent nephron progenitor compartment within the mammalian kidney. *Developmental Biology* **324**, 88–98 (2008).

106. Ouspenskaia T, Matos I, Mertz AF, Fiore VF, Fuchs E. WNT-SHH Antagonism Specifies and Expands Stem Cells prior to Niche Formation. *Cell* **164**, 156-169 (2016).

107. Tian A, Shi Q, Jiang A, Li S, Wang B, Jiang J. Injury-stimulated Hedgehog signaling promotes regenerative proliferation of Drosophila intestinal stem cells. *J Cell Biol*. **208**, 807-19 (2015).

108. Degirmenci B, Valenta T, Dimitrieva S, Hausmann G, Basler K. GLI1-expressing mesenchymal cells form the essential Wnt-secreting niche for colon stem cells. *Nature* **558**, 449-453 (2018).

109. Shin K, Lee J, Guo N, Kim J, Lim A, Qu L, Mysorekar IU, Beachy PA Hedgehog/Wnt feedback supports regenerative proliferation of epithelial stem cells in bladder. *Nature* **472**, 110-4 (2011).

110. Peng, T. *et al.* Hedgehog actively maintains adult lung quiescence and regulates repair and regeneration. *Nature* **526**, 578–582 (2015).

111. Sen GL, Reuter JA, Webster DE, Zhu L, Khavari PA. DNMT1 maintains progenitor function in self-renewing somatic tissue. *Nature* **463**, 563-7 (2010).

112. Wojcinski A, Lawton AK, Bayin NS, Lao Z, Stephen DN, Joyner AL. Cerebellar granule cell replenishment postinjury by adaptive reprogramming of Nestin^{+} progenitors. *Nat Neurosci* **20**, 1361-1370 (2017).

113. Hahn H, Christiansen J, Wicking C, Zaphiropoulos PG, Chidambaram A, Gerrard B, Vorechovsky I, Bale AE, Toftgard R, Dean M, Wainwright B. A mammalian patched homolog is expressed in target tissues of sonic hedgehog and maps to a region associated with developmental abnormalities. *J Biol Chem.* **271**, 12125-8 (1996).

114. Johnson RL, Rothman AL, Xie J, Goodrich LV, Bare JW, Bonifas JM, Quinn AG, Myers RM, Cox DR, Epstein EH Jr, Scott MP. Human homolog of patched, a candidate gene for the basal cell nevus syndrome. *Science* **272**, 1668-71 (1996).

115. i Altaba, A. R. Gli proteins and Hedgehog signaling: development and cancer. *Trends in Genetics* **15**, 418-425 (1999).

116. Wicking C, Smyth I, Bale A. The hedgehog signalling pathway in tumorigenesis and development. *Oncogene* **18**, 7844-51 (1999).

117. Ruiz i Altaba A, Sánchez P, Dahmane N. Gli and hedgehog in cancer: tumours, embryos and stem cells. *Nat Rev Cancer.* **2**, 361-72 (2002).

118. Berman DM, Karhadkar SS, Maitra A, Montes De Oca R, Gerstenblith MR, Briggs K, Parker AR, Shimada Y, Eshleman JR, Watkins DN, Beachy PA. Widespread requirement for Hedgehog ligand stimulation in growth of digestive tract tumours. *Nature* **425**, 846-51 (2003).

119. Jiang J, Hui CC. Hedgehog signaling in development and cancer. *Dev Cell* **15**, 801-12 (2008).

120. Kessler JD, Hasegawa H, Brun SN, Emmenegger BA, Yang ZJ, Dutton JW, Wang F, Wechsler-Reya RJ. N-myc alters the fate of preneoplastic cells in a mouse model of medulloblastoma. *Genes Dev.* **23**, 157-70 (2009).

121. Oh S, Huang X, Liu J, Litingtung Y, Chiang C. Shh and Gli3 activities are required for timely generation of motor neuron progenitors. *Dev Biol.* **331**, 261-9 (2009).

122. Teglund S, Toftgård R. Hedgehog beyond medulloblastoma and basal cell carcinoma. *Biochim Biophys Acta.* **1805**, 181-208 (2010).

123. Youssef KK, Van Keymeulen A, Lapouge G, Beck B, Michaux C, Achouri Y, Sotiropoulou PA, Blanpain C. Identification of the cell lineage at the origin of basal cell carcinoma. *Nat Cell Biol.* **12**, 299-305 (2010).

124. Carney TJ, Ingham PW. Drugging Hedgehog: signaling the pathway to translation. *BMC Biol.* **11**, 37 (2013).

125. Wijgerde M, McMahon JA, Rule M, McMahon AP. A direct requirement for Hedgehog signaling for normal specification of all ventral progenitor domains in the presumptive mammalian spinal cord. *Genes Dev.* **16**, 2849-64 (2002).

126. Bai CB, Stephen D, Joyner AL. All mouse ventral spinal cord patterning by hedgehog is Gli dependent and involves an activator function of Gli3. *Dev Cell* **6**, 103-15 (2004).

127. Lei Q, Zelman AK, Kuang E, Li S, Matise MP. Transduction of graded Hedgehog signaling by a combination of Gli2 and Gli3 activator functions in the developing spinal cord. *Development* **131**, 3593-604 (2004).

128. Oosterveen T, Kurdija S, Alekseenko Z, Uhde CW, Bergsland M, Sandberg M, Andersson E, Dias JM, Muhr J, Ericson J. Mechanistic differences in the transcriptional interpretation of local and long-range Shh morphogen signaling. *Dev Cell* **23**, 1006-19 (2012).

129. Stamataki D, Ulloa F, Tsoni SV, Mynett A, Briscoe J. A gradient of Gli activity mediates graded Sonic Hedgehog signaling in the neural tube. *Genes Dev.* **19**, 626-41 (2005).

130. Parker DS, White MA, Ramos AI, Cohen BA, Barolo S. The cis-regulatory logic of Hedgehog gradient responses: key roles for gli binding affinity, competition, and cooperativity. *Sci Signal* **4**, ra38 (2011).

131. Harfe BD, Scherz PJ, Nissim S, Tian H, McMahon AP, Tabin CJ. Evidence for an expansion-based temporal Shh gradient in specifying vertebrate digit identities. *Cell* **118**, 517-28 (2004).

132. Ahn S, Joyner AL. Dynamic changes in the response of cells to positive hedgehog signaling during mouse limb patterning. *Cell* **118**, 505-16 (2004).

133. Dessaud E, Yang LL, Hill K, Cox B, Ulloa F, Ribeiro A, Mynett A, Novitch BG, Briscoe J. Interpretation of the sonic hedgehog morphogen gradient by a temporal adaptation mechanism. *Nature* **450**, 717-20 (2007).

134. Balaskas N, Ribeiro A, Panovska J, Dessaud E, Sasai N, Page KM, Briscoe J, Ribes V. Gene regulatory logic for reading the Sonic Hedgehog signaling gradient in the vertebrate neural tube. *Cell* **148**, 273-84 (2012).

135. Kawagishi H, Xiong J, Rovira II, Pan H, Yan Y, Fleischmann BK, Yamada M, Finkel T. Sonic hedgehog signaling regulates the mammalian cardiac regenerative response. *J Mol Cell Cardiol.* **123**,180-184 (2018).

136. Ramalho-Santos M, Melton DA, McMahon AP. Hedgehog signals regulate multiple aspects of gastrointestinal development. *Development* **127**, 2763-72 (2000).

137. Taipale J, Beachy PA. The Hedgehog and Wnt signalling pathways in cancer. *Nature* **411**, 349-54 (2001).

138. Trapnell C, Pachter L, Salzberg SL. TopHat: discovering splice junctions with RNA-Seq. *Bioinformatics* **25**, 1105-11 (2009).

139. Trapnell C, Hendrickson DG, Sauvageau M, Goff L, Rinn JL, Pachter L. Differential analysis of gene regulation at transcript resolution with RNA-seq. *Nat Biotechnol.* **31**, 46-53 (2013).

140. Huang da W, Sherman BT, Lempicki RA. Systematic and integrative analysis of large gene lists using DAVID bioinformatics resources. *Nat Protoc*. **4**, 44-57 (2009).

141. Iacovino M, Bosnakovski D, Fey H, Rux D, Bajwa G, Mahen E, Mitanoska A, Xu Z, Kyba M. Inducible cassette exchange: a rapid and efficient system enabling conditional gene expression in embryonic stem and primary cells. *Stem Cells* **29**, 1580-8 (2011).

142. Schneider CA, Rasband WS, Eliceiri KW. NIH Image to ImageJ: 25 years of image analysis. *Nat Methods* **9**, 671-5 (2012).

143. Andrews S. (2010). FastQC: a quality control tool for high throughput sequence data. Available online at: http://www.bioinformatics.babraham.ac.uk/projects/fastqc.

144. Langmead B, Salzberg SL. Fast gapped-read alignment with Bowtie 2. *Nat Methods* **9**, 357-9 (2012).

145. Trapnell C, Williams BA, Pertea G, Mortazavi A, Kwan G, van Baren MJ, Salzberg SL, Wold BJ, Pachter L. Transcript assembly and quantification by RNA-Seq reveals unannotated transcripts and isoform switching during cell differentiation. *Nat Biotechnol.* **28**, 511-5 (2010).

146. Robinson MD, McCarthy DJ, Smyth GK. edgeR: a Bioconductor package for differential expression analysis of digital gene expression data. *Bioinformatics* **26**, 139-40 (2010).

147. Zhang Y, Liu T, Meyer CA, Eeckhoute J, Johnson DS, Bernstein BE, Nusbaum C, Myers RM, Brown M, Li W, Liu XS. Model-based analysis of ChIP-Seq (MACS). *Genome Biol*. **9**, R137 (2008).

148. Quinlan AR, Hall IM. BEDTools: a flexible suite of utilities for comparing genomic features. *Bioinformatics* **26**, 841-2 (2010).

149. Timothy L. Bailey, Mikael Bodén, Fabian A. Buske, Martin Frith, Charles E. Grant, Luca Clementi, Jingyuan Ren, Wilfred W. Li, William S. Noble. MEME SUITE:

tools for motif discovery and searching. *Nucleic Acids Research* **37**, W202-W208 (2009).

150. H. Wickham. ggplot2: elegant graphics for data analysis. Springer New York, 2009.

151. Kothary R, Clapoff S, Darling S, Perry MD, Moran LA, Rossant J. Inducible expression of an hsp68-lacZ hybrid gene in transgenic mice. *Development* **105**, 707-14 (1989).

Methods

Animal Husbandry

Mouse experiments were completed according to a protocol reviewed and approved by the Institutional Animal Care and Use Committee of the University of Chicago, in compliance with the USA Public Health Service Policy on Humane Care and Use of Laboratory Animals. The *Shh*$^{-/-}$ mouse line was obtained from the Jackson laboratory. CD1 embryos were obtained from Charles River Laboratories. *Osr1*$^{eGFPCre\text{-}ERt2}$(105) and *ROSA26*$^{Gli3T\text{-}Flag}$(95) lines were reported previously.

Embryo transcriptome profiling

The pSHF was microdissected from five individual E10.5 *Shh*$^{+/+}$ and five *Shh*$^{-/-}$ embryos, and yolk sacs were collected for genotyping. Tissues were mechanically homogenized in TRIzol Reagent (ThermoFisher Scientific 15596026), and RNA was isolated using RNeasy Mini RNA Isolation Kit (Qiagen 74104). Overall, 12µg of total RNA for each sample was treated with the mouse GLOBINclear kit (ThermoFisher Scientific AM1980) to remove the majority of globin RNA. 1ug of total RNA was then used to generate sequencing libraries using the TruSeq RNA Sample prep kit v2 (Illumina RS-122-2001), as per recommended instructions. Libraries were quantitated on an Agilent Bio-Analyzer and pooled in equimolar amounts. Pooled libraries were sequenced on the HiSeq2500 in Rapid Run Mode following the manufacturer's protocols to generate stranded single-end reads of 50bp. The number of sequenced reads per sample ranged between 11.7 million 17.7 million with an average of 15 million sequenced per sample. Quality control for raw reads involved trimming the first 13bp with FastQ Groomer to ensure a median quality

score of 36 or above for each sample. Fastq files were aligned to the UCSC mouse genome (mm9) using TopHat[138] (version 2.0.10) with the following parameters: (--segment-length 19 --segment-mismatches 2 --no-coverage-search). Between 11.4 million 17.2 million successfully mapped reads were then merged. One *Shh*$^{+/+}$ sample was discarded due to discordance with all other samples. Remaining samples were then analyzed for differential gene expression using Cuffdiff[139] (version 2.1.1) with quartile normalization. Significantly differentially expressed genes were identified using thresholds of FDR <0.05 and fold change > 1.5, resulting in 204 and 52 genes up-regulated and down-regulated, respectively, in the *Shh*$^{-/-}$ pSHF samples compared with *Shh*$^{+/+}$ samples.

The pSHF and HT from six CD1 embryos was also microdissected and RNA-seq analysis was performed to identify genes differentially expressed between the two tissues. *Shh*$^{-/-}$ dysregulated genes were then plotted on top of pSHF vs HT differentially expressed genes using R, and the distributions of *Shh*$^{-/-}$ downregulated and *Shh*$^{-/-}$ upregulated genes were compared to the distribution of all genes using Welch's two-sample T-test. Differential expression of selected genes identified by RNA-seq was validated using qPCR. RNA was harvested from *Shh*$^{+/+}$ and *Shh*$^{-/-}$ pSHF samples with a Nucleospin RNA extraction kit (Machery-Nagel 740955.250). RNA was then used to perform one-step qPCR with the iTaq One-Step system (Bio-Rad 1725151), and expression levels in mutant samples were normalized to *Shh*$^{+/+}$ samples. RNA-seq identified differentially expressed genes were also used to identify associated gene ontology (GO) terms that were enriched above a *P*-value cutoff of 0.05 using the DAVID 6.8 Functional Annotation tool[140].

Differentiation stage-dependent bioinformatic analysis

Human and mouse RNA-seq data as described in Extended Data Tables 1 & 2 were downloaded from the Encode website (www.encodeproject.org)[43]. All gene quantification files downloaded from ENCODE were grouped and each samples' FPKM was sorted and ranked with dplyr's percent rank function in R (version 3.5.1). Those files not generated by ENCODE were processed exactly according to their pipeline (https://www.encodeproject.org/rna-seq/long-rnas/). Ggplot's(3.0.0) stat_compare function was used to summarize each samples' observation for genes GLI and GAPDH. Means were compared with ANOVA, followed by a Tukey comparison of means using R base functions aov and TukeyHSD.

For state-dependent analysis, only annotated (Gencode M4, mouse and V24 human) mRNAs were kept and files were loaded into R with tximport (version 1.8) before differential expression testing with DESeq2 (version 1.20) and parameter minReplicatesForReplace set to FALSE to disallow the software from omitting samples. Differentially expressed genes from GLI1 OE and *Ptch1*$^{+/-}$ (ref. 56) Hh manipulation experiments were highlighted in a MA plot for the above experiments and the median fold change in expression was tested with ANOVA, followed by a Tukey post-hoc test. The reported $\log_2$ fold change of the manipulation experiments was plotted against the $\log_2$ fold change of the stage-dependent analysis with ggplot. Correlation was tested using R's cor.test function with the Pearson method.

For gene ontology term analysis, we used GO stats (version 2.48) hyper-geometric test on differentially expressed genes to find gene ontology terms in the Biological

Processes and KEGG pathway categories. The top 20 most significant terms by adjusted *P*-value were plotted with ggplot with the size of the points set equal to the number of genes tested divided by the number of genes in the ontology term. Color gradient was determined by the adjusted I-value of each observation.

Gli1-FTA mESC line generation

To generate an inducible GLI1 mouse embryonic stem cell (mESC) line, the coding sequence for mouse *Gli1* was inserted into the *Hprt* locus of A2Lox.cre mES cells using a method previously described[141]. Individual clones were assessed for differentiation potential and doxycycline-inducibility (data not shown). One clone was chosen and used for all experiments described herein, and all experiments were performed at the same passage number.

mESC cardiomyocyte and neuronal differentiation culture

mESCs were maintained and differentiated into cardiomyocytes as previously described[44]. RNA was collected and qPCR was performed to assess the expression of cardiac progenitor markers *Tbx5, Nkx2-5* and *Isl1*, as well as Hh markers *Gli1*, and *Ptch1* relative to *Gapdh* in differentiating cardiomyocytes. For GLI1 overexpression experiments, doxycycline (Sigma D9891, 500ng/ul) was added to cultures at the cardiac progenitor stage (Day 5). Cells were then washed and media was changed after 24hrs of exposure to doxycycline. qPCR and western blots were performed, as described above, on Day 6 samples to assess the expression level of *Gli1* and Hh targets, relative to untreated controls. Expression of the Hh target, *Foxf1*, was quantified relative to *Gapdh*

expression in cells treated with increasing concentrations of doxycycline and relative to *Gapdh* in pSHF embryo samples. Based on results from these assays, a final doxycycline concentration of 500ng/ml was chosen for all GLI1 overexpression experiments. The number of beating foci was calculated as the average number of independently beating regions within 5 fields of view across two biological samples, counted from 5 second videos taken on a Zeiss Axiovert 200m inverted widefield microscope.

Neuron differentiation was performed as previously described[52-54]. Briefly, cells were plated at a density of 9.5×10^4 /cm^2 on a 0.1% gelatin-coated dish and allowed to differentiate in N2B27 medium, which was replaced every two days. For GLI1 overexpression experiments, 500ng/ml doxycycline (Sigma D9891) was added to cultures at the neural progenitor stage (Day 3). Cells were then washed and media was changed after 48hrs of exposure to doxycycline. RNA was collected and qPCR was performed as described above to assess the expression of neural stem cell marker *Sox1*, neural progenitor marker *Nestin* and neuron marker *Tubb3,* as well as Hh markers *Gli1*, *Hhip* and *Ptch1* relative to *Gapdh* in differentiating neurons. For overexpression experiments, the relative fold change in expression of *Foxa2*, *Nestin*, *Tubb3* and *Map2* was quantified relative to control cells at each corresponding time point. The number of axons and the number of neural rosette clusters were manually counted by two independent observers blinded to the treatment from ten fields of view across two biological replicates using 10x brightfield microscopy (Olympus IX81).

mESC immunofluorescence was performed on cells from cardiac and neural differentiations, as above, with an antibody recognizing cardiac Troponin T (cTnT; 1:100; ThermoFisher Scientific MS-295-P1) and β-Tubulin III (Tubb3; 1:100; R & D Systems

MAB1195). The area of cTnT and Tubb3 positivity was calculated as the mean grey area / mm^2 of 5 fields of view across two biological replicates per condition, using the threshold measurement tool in ImageJ[142].

RNA-seq was performed on cardiac differentiations at least two replicate Day 6, Day 8 and Day 12 GLI1 OE and control samples. Data were analyzed with FastQC[143], reads were mapped to the mouse genome (mm9) with Bowtie2[144] and transcripts were assigned and quantified with Cufflinks with default parameters[145]. Reads were then normalized and differentially expressed genes for each timepoint were identified with edgeR[146]. Differentially expressed genes were then filtered to include only genes with a fold change ≥ 0.5 (log^2) and an FDR ≤ 0.05. GO term analysis on Day 6 dysregulated genes, and qPCR validation of selected genes, was performed as described above. The mean log2 fold changes of downregulated, upregulated and all genes were compared with a non-parametric Kruskall-Wallis rank sum test for Day 6, Day 8 and Day 12 samples: Day 6 chi-squared = 3804.9, df = 2, p-value < $2.2e^{-16}$; Day 8 chi-squared = 397.45, df = 2, p-value < $2.2e^{-16}$; Day 12 chi-squared = 363.78, df = 2, p-value < $2.2e^{-16}$.

Chromatin profiling

Assay for transposase-accessible chromatin was performed as previously described[89]. Briefly, the pSHF and HT were microdissected from CD1 embryos, pooled into three replicates, and dissociated with TrypLE (ThermoFisher Scientific 12605-010). For mESC samples, 150,000 cells were collected from two replicate GLI1 OE and control samples. Embryo and cell samples were then lysed, as described[89], and transposition was carried

out at 37C for 30 minutes with Illumina's Nextera DNA Library Prep kit (Illumina 15028212). Libraries were generated from transposed DNA and sequenced on an Illumina HiSeq4000 instrument in the University of Chicago's Genomic Facility. Data were analyzed with FastQC and mapped to the mouse genome (mm9) with Bowtie2 using default parameters. Peaks were called for all samples with MACS2[147] using the following parameters: -q 0.05 --nomodel --shift -100 --extsize 200 --nolambda --keep-dup all --call-summits... Peak sets from biological replicates were overlapped with the Bedtools[148] intersect tool to identify replicated peaks. Peaks sets generated from regions present in both replicates were then intersected to identify regions specific to each tissue type. For motif analysis, the summits from replicated regions were extended ±250bp, and sequence was retrieved for these regions. *De novo* and targeted motif (GLI and GLI-similar) enrichment analysis was then performed using the MEME Suite of tools[149] with a randomized or shuffled background. Pearson's correlation was calculated for read enrichment within region subsets in R and data were visualized with ggplot2[150].

Luciferase Assays

Expression vectors for mouse *Gli1*, *Gli3T* and *Tbx5*, as well as a luciferase vector containing the *Foxf1* enhancer were previously described[26]. Expression and reporter vectors were transfected into HEK293T cells using FuGENE HD (Promega E2311). Cells were cultured for 48 hours after transfection, then lysed and assayed using a Dual-Luciferase Reporter Assay system (Promega E1960).

Transient transgenics

The *Foxf1a* enhancer and minimal promoter used in the luciferase assays were subcloned from the pENTR vector into the Hsp68-LacZ vector[151] using the Gateway system (Invitrogen). GLI binding sites were mutated using the Agilent QuikChange Multi site-directed mutagenesis kit (Agilent 210515-5). The resulting constructs were digested with NotI enzyme to remove the pBlueScript backbone, gel-purified, injected into fertilized mouse eggs at the University of Chicago Transgenics Core Facility and implanted into female mice. Five embryos were harvested at E9.5 and stained as described previously[25].

Embryo Immunohistochemistry / Immunofluorescence

E10.5 embryos were harvested from timed pregnancies and yolk sacs were collected for genotyping. Embryos were fixed overnight in 4% paraformaldehyde, washed with PBS and processed for paraffin sectioning. 5um serial sections were generated and used for immunofluorescence with primary antibodies recognizing sarcomeric myosin (1:20; DSHB MF20) and Alexa Fluor-conjugated secondary antibodies (1:1000; ThermoFisher Scientific). Antigen retrieval was performed on all sections with 10mM sodium citrate buffer. DAPI was used to counterstain tissues and provide a tissue reference. Sections were imaged with an Olympus IX81 inverted widefield microscope using 10x and 20x objectives in the University of Chicago's Integrated Light Microscopy Core Facility. Images were processed with ImageJ.

Histology

Activation of *CreER*^{T2} was accomplished by intraperitoneal injection with 2 mg tamoxifen (TM) per dose in corn oil to pregnant dams, as previously described[25]. Pregnant

ROSA26$^{Gli3T\text{-}Flag\ c/c}$ females were dosed at E7.5, E8.5 and E9.5, and histological studies were performed at E14.5. Embryos were harvested and fixed in 4% paraformaldehyde overnight at 4ºC, and then processed for paraffin sectioning. 5um sections were then stained with hematoxylin and eosin to reveal the structural morphology of the atrial septum in mutant and control embryos.

Author contributions

M.R. designed and performed the experiments and wrote the manuscript. A.D.H., J.D.S., A.G., S.L., N.D., E.L. and J.J-L. performed *in vivo* experiments. C.K., S.Y., E.H., and E.L. performed *in vitro* experiments. X.H.Y., C.P-C. and K.I. performed computational analyses. S.S-K.C. and M.K. generated the GLI1-FTA mESC line. D.J.G. designed the experiments. I.P.M. designed the experiments and wrote the manuscript.

Competing Interests

The authors report no competing interests.

Figures

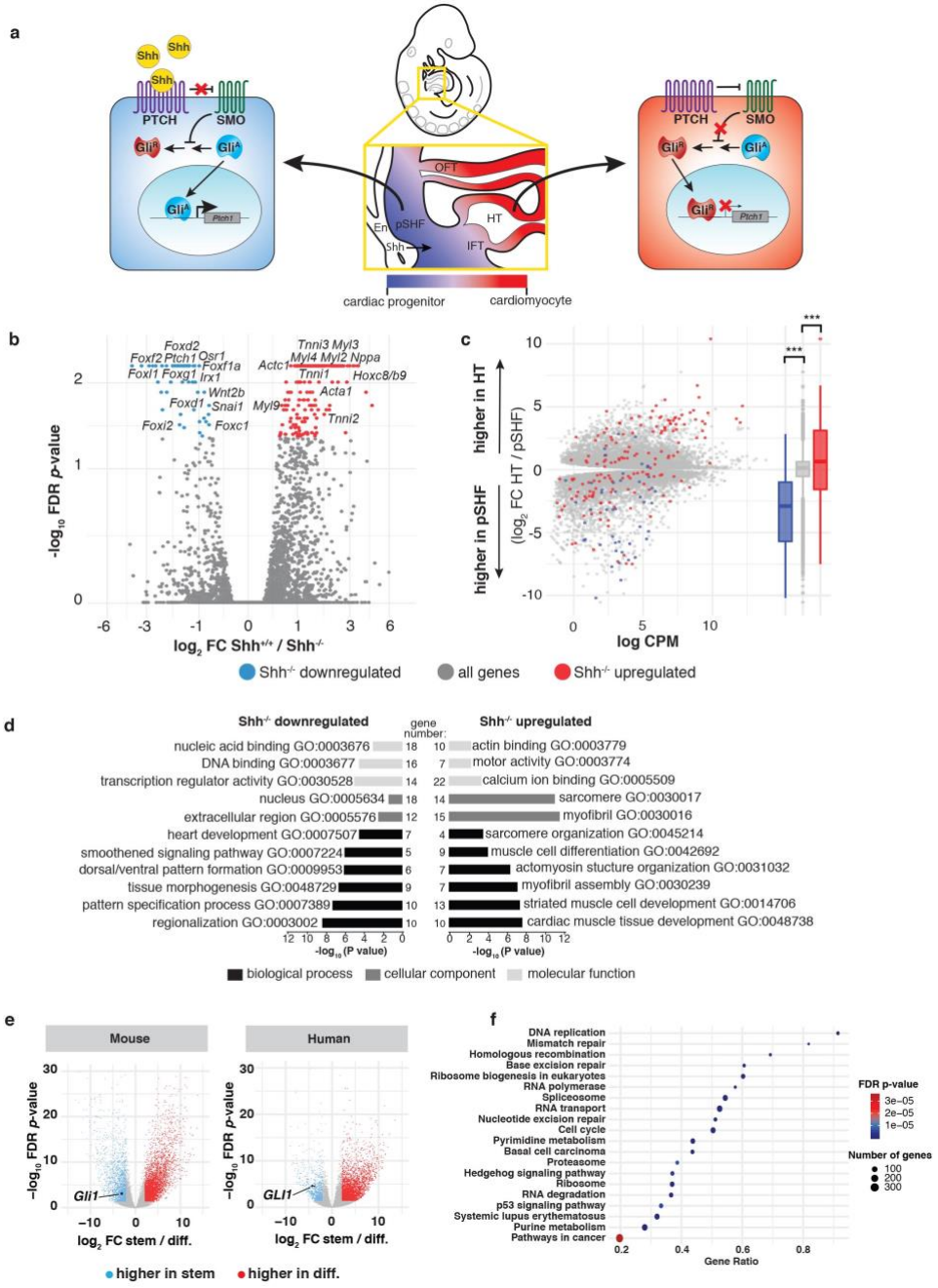

Figure 1. Hedgehog signaling activates a progenitor gene regulatory network, and represses the differentiation program, during cardiac development. **a,** Schematic of cardiac progenitors (blue) in the E10.5 pSHF and differentiating cardiomyocytes (red) in the HT, sagittal view. Active Hh signaling in the pSHF leads to

accumulation of GLI^A in the nucleus and the activation of Hh target genes, such as *Ptch1*, in cardiac progenitors (left). Inactive Hh signaling results in the truncation of GLI^A to GLI^R and accumulation of the repressor in the nuclei of differentiating cardiomyocytes (right). **b**, Volcano plot displaying upregulated and downregulated genes in the $Shh^{-/-}$ pSHF. Red is upregulated, blue is downregulated. **c**, MA plot and box plots illustrating the distribution of $Shh^{-/-}$ dysregulated genes in the context of differential expression between the wild type pSHF and HT. ANOVA for three groups: *F-value* = 246.2, *P-value* < $2e^{-16}$; post-hoc Pairwise T-test with Benjamini-Hochberg correction: upregulated vs all genes *P-value* = $1e^{-12}$, downregulated vs all genes P-value < $2e^{-16}$, downregulated vs upregulated *P-value* < $2e^{-16}$. **d**, Gene ontology (GO) analysis of $Shh^{-/-}$ dysregulated genes. **e**, Gene expression rankings for *Gli1/GLI1* and *Gapdh/GAPDH* in human and mouse differentiation series. ANOVA for *Gli1* rank in three mouse groups: F-value = 11.4, *P-value* = $1.15e^{-4}$; post-hoc Tukey Test: stem vs progenitor *P-value* = 0.14, stem vs differentiated *P-value* = $1.56e^{-4}$, progenitor vs differentiated *P-value* = $1.39e^{-3}$. ANOVA for *Gapdh* rank in three human groups: *F-value* = 3.99, *P-value* = 0.03. ANOVA for *GLI1* rank in three human groups: *F-value* = 20.3, *P-value* = $1.25e^{-6}$; post-hoc Tukey Test: stem vs progenitor *P-value* = $1.70e^{-4}$, stem vs differentiated *P-value* = $7.0e^{-7}$, progenitor vs differentiated *P-value* = 0.12. ANOVA for *GAPDH* rank in three human groups: *F-value* = 1.60, *P-value* = 0.22. **f,** Volcano plots displaying differentially expressed genes between the stem and differentiated cell states for mouse and human. Mouse *Gli1*: FC = -2.99, $-\log_{10}$ FDR *P-value* = $8.45e^{-4}$. Human *GLI1*: FC = -3.80, $-\log_{10}$ FDR *P-value* = $3.06e^{-5}$. (* P-value ≦ 0.05, ** P-value ≦ 0.01, *** P-value ≦ 0.01).

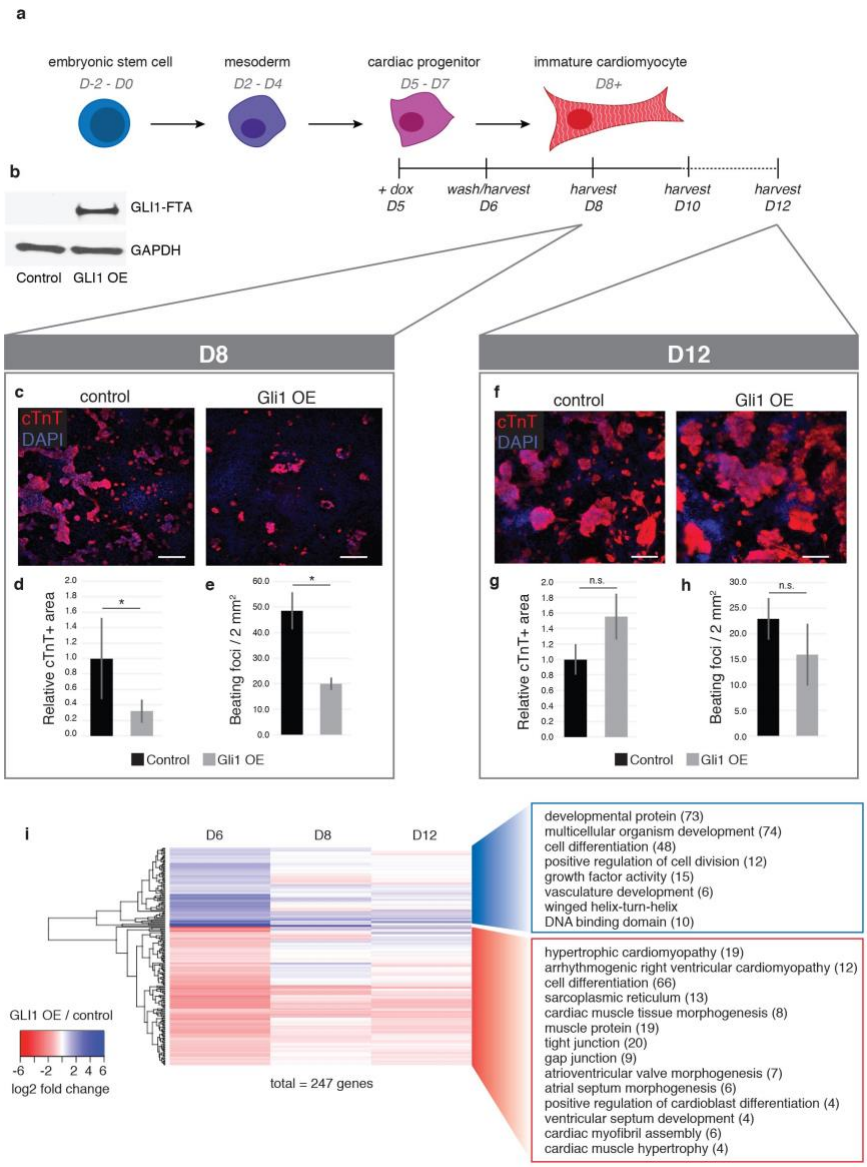

Figure 2. GLI^{A} expression in cardiac progenitors delays cardiomyocyte differentiation. **a**, Schematic representation of the GLI1 OE experimental design employed in mESC-derived differentiating cardiomyocytes. **b**, Normally Hh-inactive cardiac progenitors express GLI1 protein after doxycycline treatment for 24 hours, as assessed by western blot. **c**, Immunofluorescent staining for cardiac troponin (cTnT) in control and GLI1 OE cells harvested at Day 8. **d**, Quantification of the area of cTnT-positivity in control and GLI1 OE cells at Day 8. **e**, Quantification of the number of beating

foci in videos taken of control and GLI1 OE cells at Day 8. **f**, Immunofluorescent staining for cardiac troponin in control and GLI1 OE cells harvested at Day 12. **g**, Quantification of the area of cTnT-positivity in control and GLI1 OE cells at Day 12. **h**, Quantification of the number of beating foci in videos taken of control and GLI1 OE cells at Day 12. **i**, Differential gene expression time series and GO analyses of GLI1 OE cells. GO terms shown are those associated with development and differentiation from gene dysregulated at Day 6. Scale bars in **c**,**f** = 100um. (* P-value ≦ 0.05, ** P-value ≦ 0.01, *** P-value ≦ 0.01).

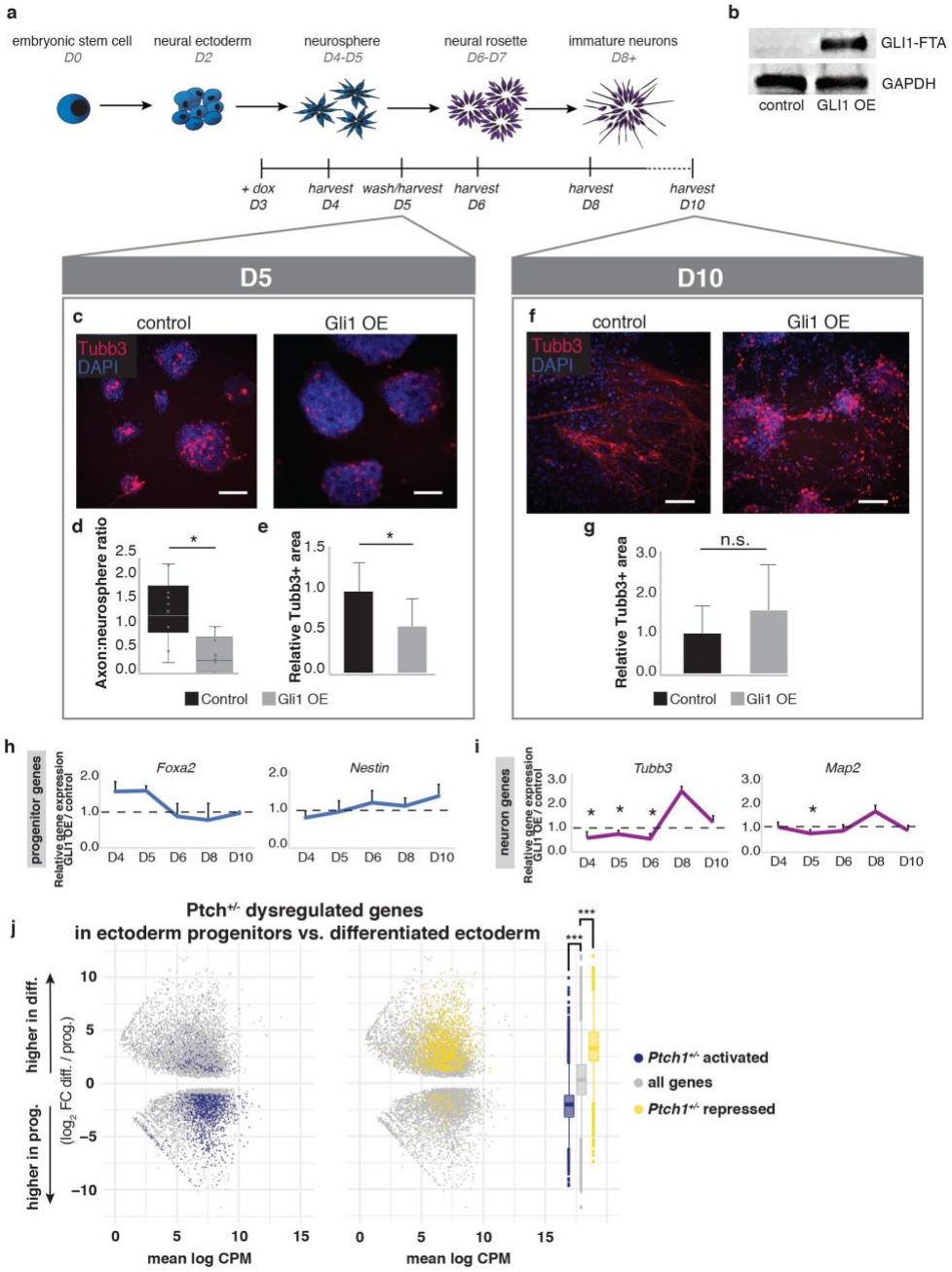

Figure 3. GLI^{A} expression in neuronal progenitors delays neuron differentiation. **a**, Schematic representation of the GLI1 OE experimental design employed in mESC-derived differentiating neurons. **b**, Neuronal progenitors with low levels of endogenous Hh activity express GLI1 protein after doxycycline treatment for 24 hours, as assessed by western blot. **c**, Immunofluorescent staining for pan-neuronal

marker Tubb3/TUJ1 in control and GLI1 OE cells harvested at Day 5. **d**, Quantification of the ratio of axons to neurospheres in control and GLI1 OE cells at Day 5. **e**, Quantification of the area of Tubb3-positivity in control and GLI1 OE cells at Day 5. **f**, Immunofluorescent staining for pan-neuronal marker Tubb3/TUJ1 in control and GLI1 OE cells harvested at Day 10. **g**, Quantification of the area of Tubb3-positivity in control and GLI1 OE cells at Day 10. **h**, qPCR validation of temporary upregulation of neuronal progenitor-specific genes in GLI1 OE cells. **i**, qPCR validation of temporary downregulation of differentiating neuron-specific genes in GLI1 OE cells. **j**, Correlation plot comparing *Ptch1*$^{+/-}$ dysregulated fold changes to the fold changes of genes differentially expressed between ectodermal progenitors and differentiated ectoderm stages. Pearson correlation r = -0.71, *P-value* = < $2e^{-16}$. **k**, MA plot and box plots illustrating the distribution of *Ptch1*$^{+/-}$ dysregulated genes in the context of differential expression between ectodermal progenitors and differentiated ectoderm stages. ANOVA for three groups: *F-value* = 1557.0, *P-value* = < $2e^{-16}$; post-hoc Tukey Test: upregulated vs all genes *P-value* < $2e^{-16}$, downregulated vs all genes P-value < $2e^{-16}$, downregulated vs upregulated *P-value* < $2e^{-16}$. Scale bars in **c**,**f** = 100um. (* P-value ≦ 0.05, ** P-value ≦ 0.01, *** P-value ≦ 0.01).

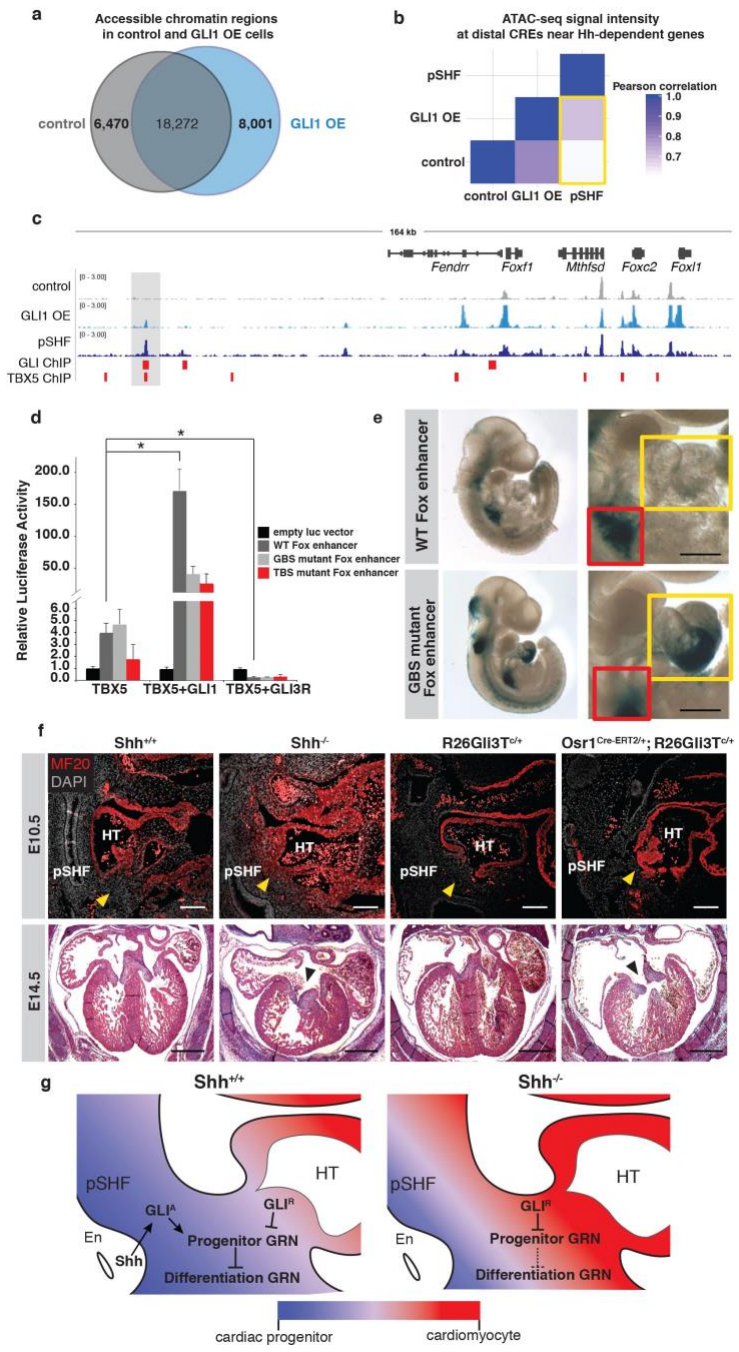

Figure 4. GLI^{A} expression leads to remodeled chromatin at distal CREs near progenitor-specific genes and act as a biphasic switch to control progenitor gene expression and the timing of differentiation. a, Venn diagram showing the number of common and specific accessible chromatin regions in GLI1 OE cells and control cells. **b**. Pearson correlation between ATAC-seq read intensity within regions containing a GLI

motif near Hh-dependent genes in pSHF, GLI1 OE and control samples. Gold box highlights the difference between the correlation coefficients for control-pSHF and GLI1 OE-pSHF comparisons. Control-pSHF *r* = 0.61, GLI1 OE-pSHF *r* = 0.71. **c,** ATAC-seq read enrichment and GLI/TBX5 ChIP-seq peaks[95,100] at a putative regulatory element upstream of the Hh-dependent *Foxf1* target in pSHF, GLI1 OE and control samples. d, Luciferase reporter activity modulated by GLI^A and GLI^R at wild type and GBS/TBS mutant *Foxf1* enhancers, in cooperation with TBX5. **e**, Transient transgenic analysis of *lacZ* reporter expression in the pSHF (red box) and HT (gold box) driven by wild type and GBS mutant versions of the *Foxf1* CRE. **f**. Immunofluorescent staining for MF20 (sarcomeric myosin) in the E10.5 pSHF of control and Hh mutant embryos (grey = DAPI, red = MF20), and histological sections of E14.5 hearts from control and Hh mutant embryos. Yellow arrowheads demarcate mesenchymal cardiac progenitors migrating into the HT at the posterior aspect of the inflow tract, and black arrowheads highlight incidence of AVSD. **g**, Model depicting the Hh-dependent activation of a progenitor gene regulatory network in the embryonic pSHF by GLI^A and repression of the progenitor transcription factor network in the HT by GLI^R. In Hh mutant embryos, the progenitor network is not activated and precocious differentiation of cardiomyocytes is permitted, resulting in severe cardiac defects. Scale bars in **e** = 100um, **f** = 200um. (* P-value ≦ 0.05, ** P-value ≦ 0.01, *** P-value ≦ 0.01).

Extended Data Figures

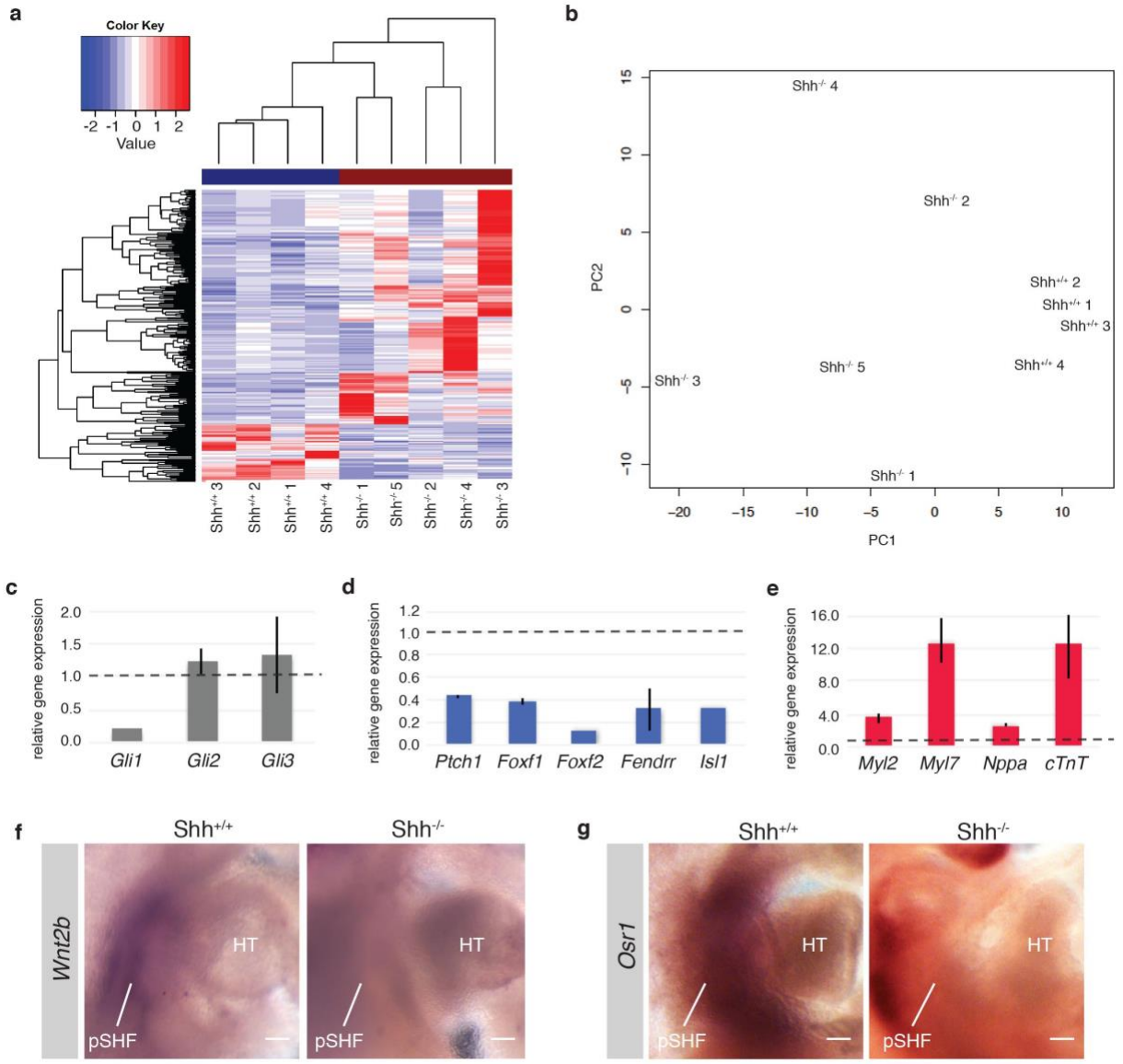

Extended Data Figure 1. Differential gene expression analysis reveals downregulation of progenitor genes expressed in the SHF. a, Heatmap showing differentially expressed genes in $Shh^{+/+}$ and $Shh^{-/-}$ replicate samples. **b**, PCA plot of differentially expressed genes demonstrating that genotype accounts for the highest proportion of variation among embryo gene expression profiles. **c**, qPCR validation of reduced Hh activation in the *Shh*$^{-/-}$ pSHF. **d**, qPCR validation of downregulated progenitor

genes in the *Shh*$^{-/-}$ pSHF. **e**, qPCR validation of upregulated cardiomyocyte genes in the *Shh*$^{-/-}$ pSHF. **f**, *In situ* hybridization of *Wnt2b* in the SHF of *Shh*$^{+/+}$ and *Shh*$^{-/-}$ embryos demonstrating pSHF-specific loss of gene expression. **g**, *In situ* hybridization of *Osr1* in the SHF of *Shh*$^{+/+}$ and *Shh*$^{-/-}$ embryos demonstrating pSHF-specific loss of gene expression. Scale bar = 100um.

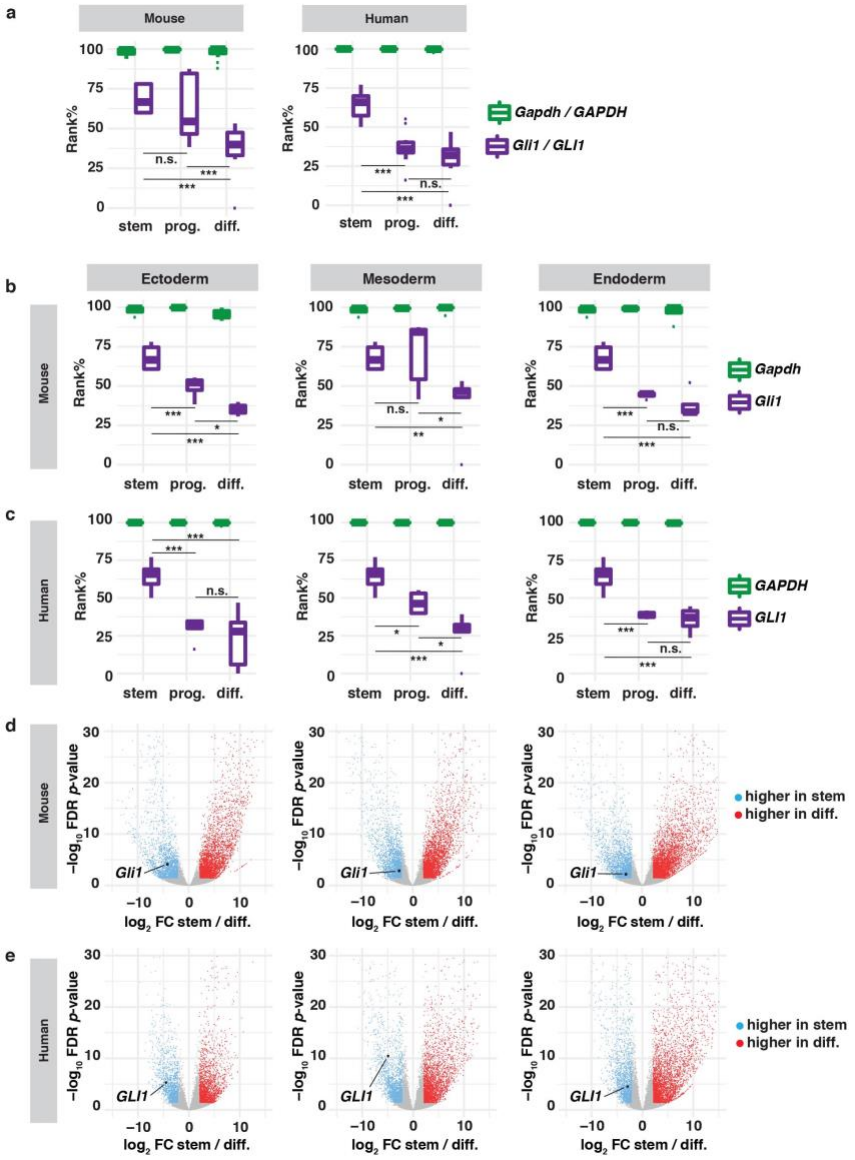

Extended Data Figure 2. Hedgehog signaling is highest in stem and progenitor cell states, and lowest in differentiated cell states in tissues from all three developmental germ layers. a, Gene expression rankings for *Gli1* and *Gapdh* in mouse germ layer-specific differentiation series. ANOVA for *Gli1* rank in ectoderm: F-value = 22.86, *P-value* = $3.89e^{-5}$; mesoderm: F-value = 5.25, *P-value* = 0.01; endoderm: F-value = 24.73, *P-value* = $5.54e^{-5}$. ANOVA for *Gapdh* rank in ectoderm: *F-value* = 3.24, *P-value* = 0.07; mesoderm: *F-value* = 2.07, *P-value* = 0.15; endoderm: *F-value* = 0.55, *P-*

value = 0.59. **b**, Gene expression rankings for *GLI1* and *GAPDH* in human germ layer-specific differentiation series. ANOVA for *GLI1* rank in ectoderm: F-value = 17.33, *P-value* = $1.26e^{-4}$; mesoderm: F-value = 21.77, *P-value* = $3.67e^{-5}$; endoderm: F-value = 21.28, *P-value* = $1.13e^{-4}$. ANOVA for *GAPDH* rank in ectoderm: *F-value* = 1.17, *P-value* = 0.34; mesoderm: *F-value* = 0.32, *P-value* = 0.73; endoderm: *F-value* = 2.32, *P-value* = 0.14. **c,** Volcano plots displaying differentially expressed genes between the stem and differentiated cell states for mouse germ layer-specific datasets. *Gli1* in ectoderm: FC = -4.13, $-\log_{10}$ FDR *P-value* = $7.45e^{-5}$; mesoderm: FC = -2.61, $-\log_{10}$ FDR *P-value* = $1.37e^{-3}$; endoderm: FC = -3.12, $-\log_{10}$ FDR *P-value* = $6.27e^{-3}$. **d,** Volcano plots displaying differentially expressed genes between the stem and differentiated cell states for human germ layer-specific datasets. *GLI1* in ectoderm: FC = -4.47, $-\log_{10}$ FDR *P-value* = $5.74e^{-6}$; mesoderm: FC = -4.93, $-\log_{10}$ FDR *P-value* = $3.99e^{-11}$; endoderm: FC = -2.95, $-\log_{10}$ FDR *P-value* = $3.63e^{-5}$. **e**, Gene ontology term dot plot for genes downregulated in the mouse differentiated cell state, relative to the progenitor cell state. (* P-value ≦ 0.05, ** P-value ≦ 0.01, *** P-value ≦ 0.01).

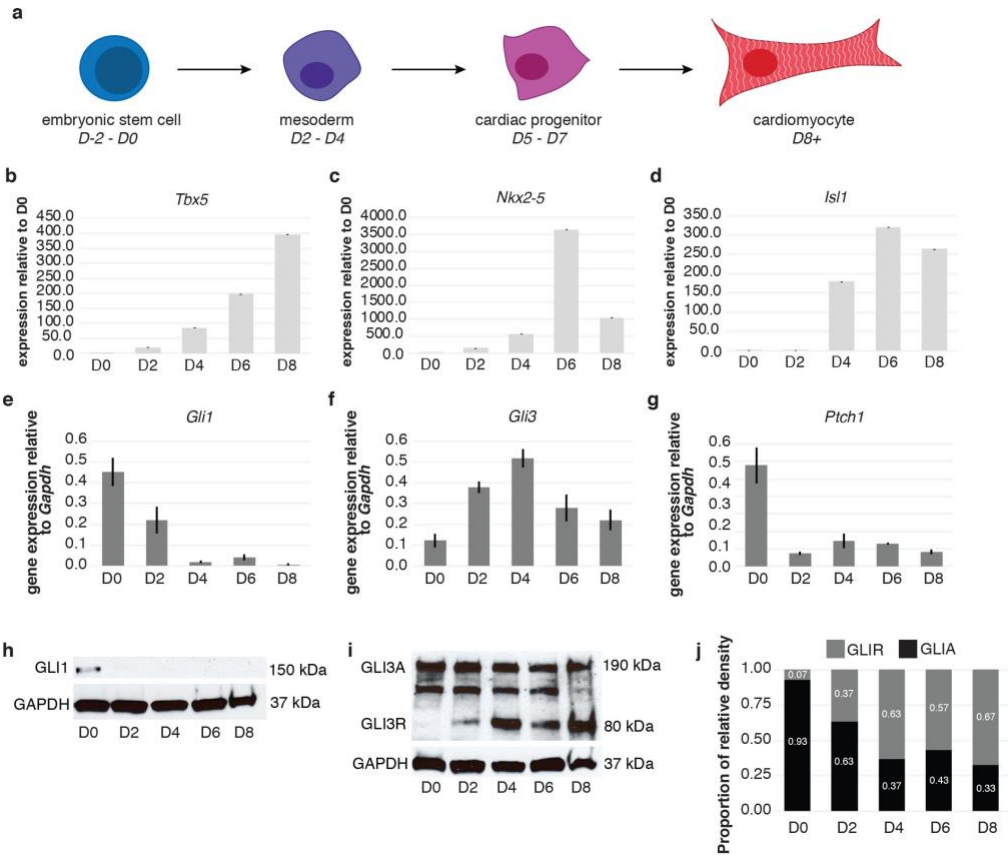

Extended Data Figure 3. Hedgehog signaling is inactive during mESC-derived cardiomyocyte differentiation. **a**, Schematic depicting the *in vitro* cardiomyocyte differentiation system employed in these studies. **b**, Expression level of cardiac lineage determining transcription factor *Tbx5* throughout the differentiation time series. **c**, Expression level of *Nkx2-5* throughout the differentiation time series. **d**, Expression level of *Isl1* throughout the differentiation time series. **e**, Expression level of *Gli1*, relative to *Gapdh*, during cardiomyocyte differentiation. **f**, Expression level of *Gli3*, relative to *Gapdh*, during cardiomyocyte differentiation. **g**, Expression level of the Hh target *Ptch1*, relative to *Gapdh*, during cardiomyocyte differentiation. **h**, Western blot demonstrating the expression level of GLI1 protein during cardiomyocyte differentiation. **i**, Western blot demonstrating the expression level of $GLI3^A$ and $GLI3^R$ protein during

cardiomyocyte differentiation. **j**, Relative proportions of GLI^A and GLI^R proteins expressed during cardiomyocyte differentiation.

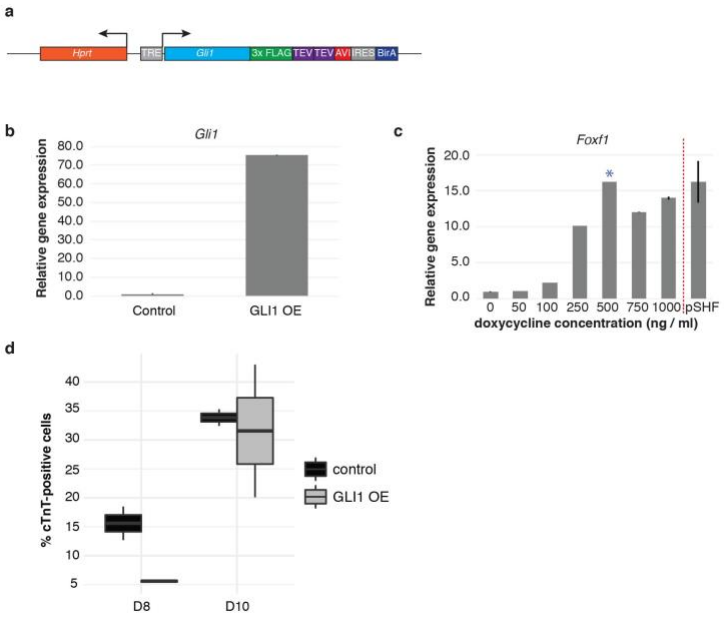

Extended Data Figure 4. GLI1 overexpression in cardiac progenitors leads to activation of pSHF Hedgehog targets. **a**, Schematic representation of the *Gli1-FTA* transgenic cassette inserted into the *Hprt* locus in mESCs. **b**, 500ng/ml doxycycline treatment of the *Gli1-FTA* transgenic line for 24 hours results in robust activation of *Gli1* transcript. **b**, Expression levels of the Hh target *Foxf1*, relative to *Gapdh*, resulting from various doxycycline concentrations in cardiac progenitors, as compared to endogenous *Foxf1* and *Gapdh* expression levels in the embryonic pSHF. **d**, Percentage of cTnT+ control and GLI1 OE samples at D8 and D10 of differentiation, as measured by fluorescence-activated cell sorting. (* P-value ≦ 0.05, ** P-value ≦ 0.01, *** P-value ≦ 0.01).

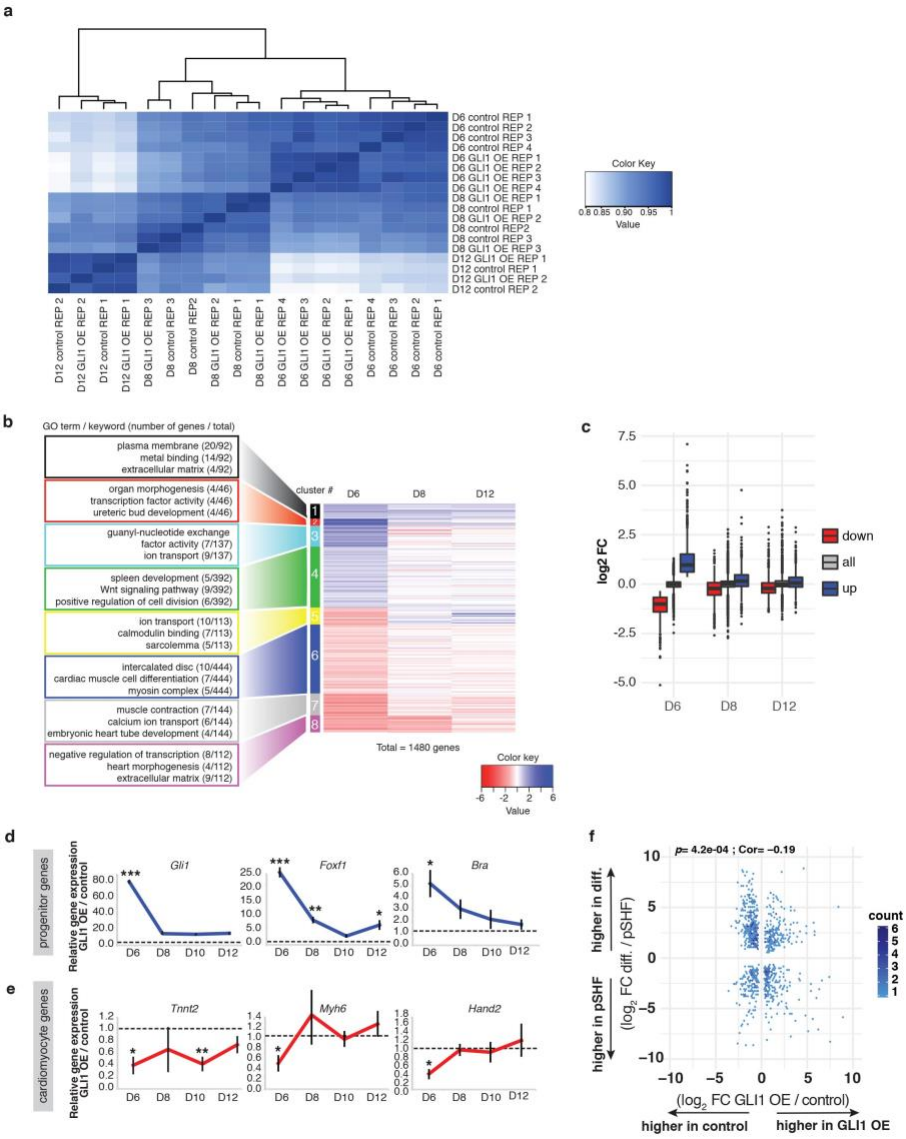

Extended Data Figure 5. Brief GLI1 overexpression in cardiac progenitors results in a transient disruption to the cardiomyocyte differentiation program. **a**, Heatmap displaying correlation of gene expression profiles from GLI1 OE and control cells at all differentiation stages analyzed. Clustering of samples reveals a strong separation of samples by treatment at Day 6, but intercalation of treated with untreated samples at Day 8 and Day 12. **b**, Heatmap time series of genes differentially expressed at Day 6 demonstrates a trend towards normalization of gene expression as differentiation

proceeds and cells recover from GLI1 OE. Gene ontology (GO) term analysis reveals that gene clusters containing genes that are transiently upregulated at Day 6 associate with progenitor-related GO terms, while clusters containing genes that are transiently downregulated at Day 6 associate with cardiomyocyte-differentiation related GO terms. **c**, Time series of the mean $\log_2$ fold change of genes downregulated and upregulated at Day 6, and their fold changes at Day 8 and Day 12, relative to all genes. **d**, qPCR validation of a temporary downregulation of progenitor-specific genes in GLI1 OE cells. **e**, qPCR validation of a temporary upregulation of cardiomyocyte-specific genes in GLI1 OE cells. (* P-value ≦ 0.05, ** P-value ≦ 0.01, *** P-value ≦ 0.01).

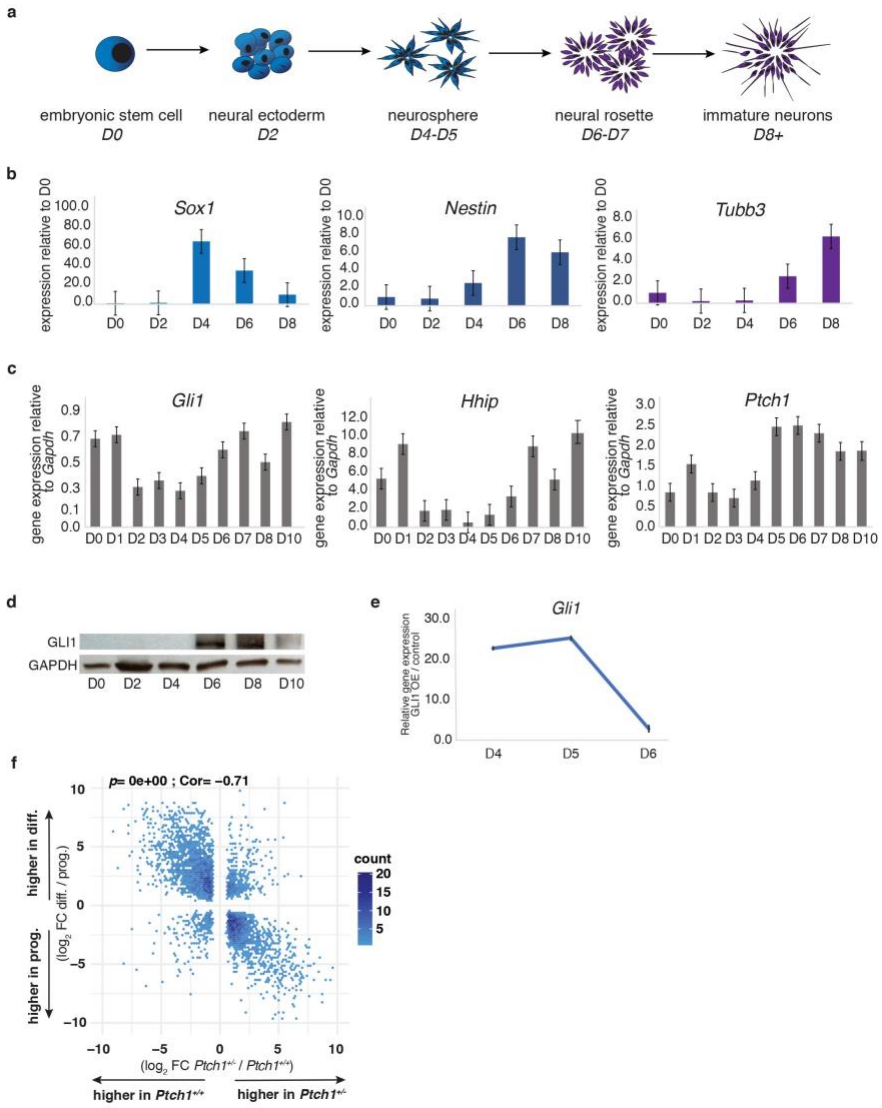

Extended Data Figure 6. Hedgehog signaling is lowest in mESC-derived progenitors during neuronal differentiation. **a**, Schematic depicting the *in vitro* neuronal differentiation system employed in these studies. **b**, Time series of expression levels of neuronal lineage stage-specific markers of differentiation. **c**, Expression level of *Gli1*, *Hhip* and *Ptch1* relative to *Gapdh*, during neuronal differentiation. **d**, Western blot demonstrating the expression level of GLI1 protein during neuronal differentiation. **e**, 500ng/ml doxycycline treatment of the *Gli1-FTA* transgenic line for 48 hours results in

robust activation of *Gli1* transcript, which then returns to control levels by 24 hours after doxycycline removal.

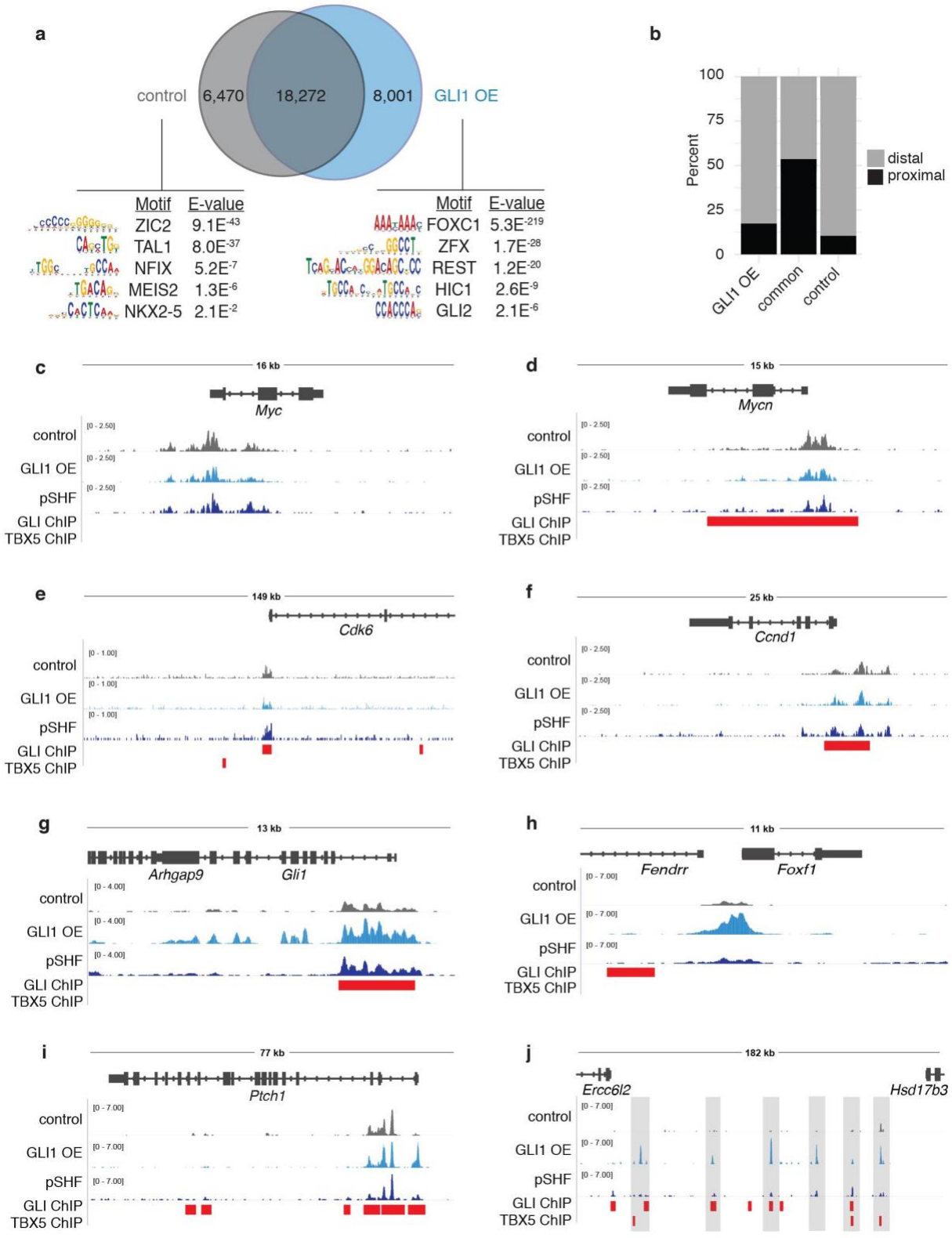

Extended Data Figure 7. Brief GLI1 overexpression in cardiac progenitors results increased chromatin accessibility near Hh-dependent genes. **a**, Venn diagram showing common and specific accessible chromatin regions in GLI1 OE cells and control cells, and TF motifs enriched in each specific subset. **b**, Stacked bar graph depicting the location of accessible regions relative to the closest TSS of all tissue-specific peaks (proximal is ≤ 1.5kb; distal is ≥ 1.5kb). **c-f**, ATAC-seq read enrichment and ChIP-seq peaks at the promoters of cell cycle regulators *Myc* (**c**), *Mycn* (**d**), *Cdk6* (**e**) and *Ccnd1* (**f**) in GLI1 OE and control cells, as well as SHF cardiac progenitors. **g-i**, ATAC-seq read enrichment and ChIP-seq peaks at the promoter of the Hh targets *Gli1* (**g**), *Foxf1* (**h**) *and Ptch1* (**i**) in GLI1 OE and control cells, as well as SHF cardiac progenitors. **j**, ATAC-seq read enrichment and GLI ChIP-seq binding regions at a putative regulatory locus upstream of *Ptch1* in GLI1 OE and control cells, as well as SHF cardiac progenitors. Grey boxes indicate regions of increased accessibility upon GLI1 OE that also have enrichment in pSHF samples.

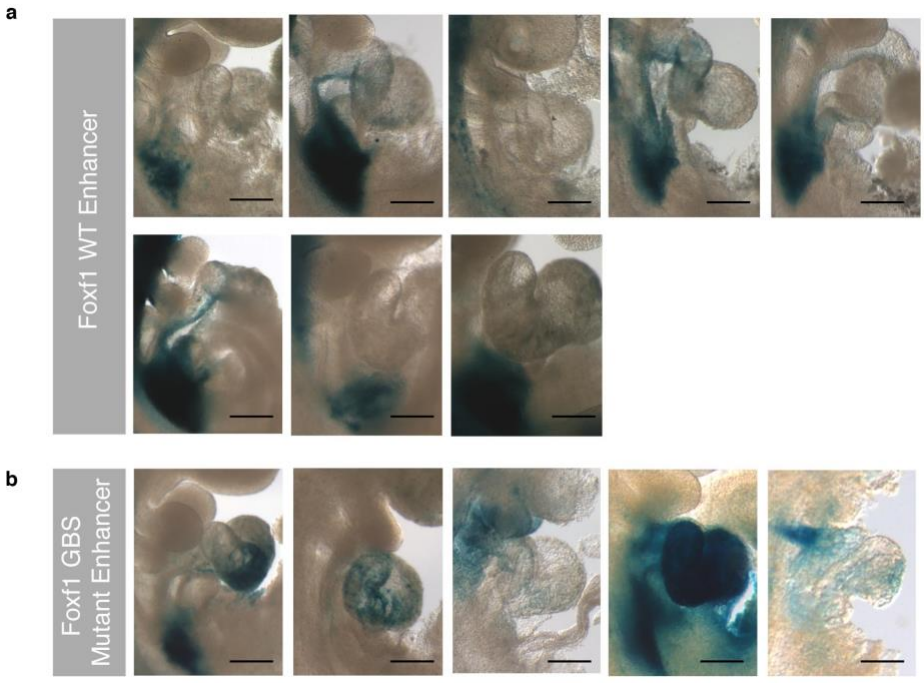

Extended Data Figure 8. GLI binding sites are required for progenitor-specific activity of a distal CRE upstream of Hh-dependent SHF genes. a, transient transgenic analysis of embryos injected with the Hsp68-LacZ vector under the control of the WT *Foxf1* enhancer. **b**, transient transgenic analysis of embryos injected with the Hsp68-LacZ vector under the control of the GBS mutant *Foxf1* enhancer. Scale bar in **a**, **b** = 100um.

ED Table 1. Mouse datasets used for bioinformatic analyses of stage-dependent gene expression.

Stage	Germ Layer	Tissue Type	Number of Replicates	GEO Series	Reference PMID
Stem		ES-Bruce4	2	GSE93453	22955616
		AN3-12	3	GSE99977	28945705
		C57BL/6-129	2	GSE99521	29224777
Progenitor	*Ectoderm*	E7.5 Ectoderm	2	GSE76505	29203909
		E10.5 Forebrain	2	GSE88173	22955616
		E10.5 Hindbrain	2	GSE88662	22955616
		E11.5 Neural Tube	2	GSE78370	22955616
	Mesoderm	E7.5 Mesoderm	2	GSE76505	29203909
		E8.5 Mesoderm	3	N/A	Unpublished (IM)
		E10.5 SHF	6	N/A	This manuscript
		E10.5 Limb Bud	2	GSE88680	22955616
	Endoderm	E7.5 Endoderm	2	GSE76505	29203909
		E11.5 Liver	2	GSE78357	22955616
Differentiated	*Ectoderm*	Brain	2	GSE93496	22955616
	Mesoderm	Heart	2	GSE93483	22955616
		Skeletal Muscle	2	GSE78487	22955616
		Adipose Tissue	2	GSE90193	22955616
	Endoderm	Sigmoid Colon	2	GSE93495	22955616
		Liver	2	GSE90180	22955616

ED Table 2. Human datasets used for bioinformatic analyses of stage-dependent gene expression.

Stage	Germ Layer	Tissue Type	Number of Replicates	GEO Series	Reference PMID
Stem		H1-hESC	2	GSE16256	19829295
		HUES64	2	GSE17312	20944595
		UCSF-4	2	GSE16368	25690954
Progenitor	*Ectoderm*	Ectodermal Cell	2	GSE17312	20944595
		Neurosphere	2	GSE16368	20944595
		Neural Stem Progenitor Cell	2	GSE16256	19829295
	Mesoderm	Mesendoderm	2	GSE16256	19829295
		Mesodermal Cell	2	GSE17312	20944595
	Endoderm	Endodermal Cell	2	GSE17312	20944595
		Large Intestine	1	GSE18927	20944595
Differentiated	*Ectoderm*	Neural Cell	2	GSE78640	22955616
		Bipolar Neurons	2	GSE87963	22955616
		Brain	2	GSE93490	22955616
	Mesoderm	Aorta	2	GSE16256	19829295
		Psoas Muscle	2	GSE16256	19829295
		Cardiomyocyte	2	GSE88167	22955616
		Heart	2	GSE93498	22955616
	Endoderm	Hepatocytes	2	GSE88601	22955616
		Sigmoid Colon	2	GSE16256	19829295
		Liver	2	GSE93481	22955616